Accelerating expansion or inhomogeneity? A comparison of the ΛCDM and Lemaître – Tolman models

Andrzej Krasiński
N. Copernicus Astronomical Centre,
Polish Academy of Sciences,
*Bartycka 18, 00 716 Warszawa, Poland**
(Dated:)

It is shown how certain observations interpreted in the background of the Friedmann model with $\Lambda < 0 = k$ (the ΛCDM model) can be re-interpreted using the $\Lambda = 0$ Lemaître – Tolman (L–T) model so as to do away with the "dark energy". The purpose of the paper is to clarify the underlying geometrical relations by doing the calculations as much as possible analytically or by very simple numerical programs. In the first part of the paper (fictitious) observations of the distribution of expansion velocity along the past light cone of the observer are considered. It is shown that the whole past light cone of the ΛCDM observer can be reproduced in the L–T model with $\Lambda = 0 = E$. This is a geometric exercise that has the advantage of being free of numerical complications. In the second part, the luminosity distance – redshift relation of the ΛCDM model is duplicated using the L–T model with $-k = 2E/r^2 = \text{constant} > 0$. The value of k and the function $t_B(r)$ are determined by the ΛCDM parameters. General properties of this L–T model are described. Difficulties of carrying the numerical calculations through the apparent horizon are presented in detail and mostly solved. The second model is a counterexample to the claim that an L–T model mimicking ΛCDM must contain a void around the center – it has a peak of density at $R = 0$.

PACS numbers:
Keywords:

I. ACCELERATING EXPANSION OR INHOMOGENEITY?

As is well-known by now, in the years 1998 – 1999 two teams of observers [1, 2] concluded that the observed peak luminosity of the type Ia supernovae is smaller than was implied by a $\Lambda = 0$ Friedmann model. An elaborate fitting procedure led to the conclusion that the best-fit model *within the Robertson – Walker (RW) class with zero pressure* is the one with the curvature index $k = 0$ and a value of the cosmological constant that accounts for $\approx 68\%$ of the current energy-density of the Universe [3], now called the ΛCDM model. Thus, at present, the Universe should be expanding at an accelerating rate. The substance that causes this acceleration was named "dark energy". Strange as it is (an observed effect being caused by an entity that no-one has ever seen outside this cosmological context), this hypothesis was almost universally accepted, and the existence of the dark energy is now taken for granted by nearly all authors.

Meanwhile, it has been demonstrated in several papers that if one gives up on the homogeneity assumption, then even the simplest among the realistic inhomogeneous models, the Lemaître [4] – Tolman [5] (L–T) model, can account for the apparent dimming of the type Ia supernovae using a suitable inhomogeneous distribution of mass in the Universe, with zero cosmological constant and decelerated expansion. Among the first papers that introduced this alternative description was the one by Iguchi, Nakamura and Nakao [6]. Later, it was demonstrated by examples that when the L–T model is employed at full generality, with no a priori simplifying assumptions, then two sets of observational data can be reproduced, for example the pairs (angular diameter distance – mass density in the redshift space) and (angular diameter distance – expansion rate) [7].

Those earlier considerations resorted to numerical calculations almost from the beginning, which obscured the underlying geometrical relations. In the present paper, a comparison of the ΛCDM model with the $\Lambda = 0$ L–T model is done by more transparent means. Explicit algebraic and differential equations are used almost exclusively, and several properties of the L–T model thus adapted are determined by exact calculations.

In the first part of the paper (Sections IV – VII) the distribution of the cosmic expansion velocity along the past light cone of the observer is considered. It is shown that, with a suitably chosen bang-time function $t_B(r)$, the central observer in the L–T model with $E = 0 = \Lambda$ can see *the same* past light cone as an observer in the ΛCDM model. This proof is unrelated to actual problems of observational cosmology, but it is free of numerical complications, and therefore is presented first.

In the second part (Sections VIII – XVIII), the luminosity distance – redshift relation, $D_L(z)$, of the ΛCDM model is duplicated in the L–T model with $\Lambda = 0$ and $-k = 2E/r^2 = \text{constant} > 0$ (this is the same k as in the limiting Friedmann model). The value of k is determined by fine-tuning the values of redshift at the origin and at the apparent horizon, and the effect of Λ is reproduced by the L–T bang time function $t_B(r)$.

The L–T model mimicking the ΛCDM $D_L(z)$ relation

*Electronic address: akr@camk.edu.pl

is determined for a single instant of observation. The time-evolution of the two models is different, and they can be distinguished by observations that are sensitive to time-changes rather than just to an instant snapshot of the Universe, for example by the redshift drift [8].

The approach used here leads to a few clarifications. Among other things, it is shown how the obstacles to carrying the numerical integration through the apparent horizon, reported in Refs. [6, 9] (and incorrectly interpreted in [9] as a "pathology" of the L–T model), can be overcome. Also, the model considered in the second part provides a counterexample to the claim that an L–T model mimicking accelerated expansion must contain a void around its center of symmetry.

II. A QUICK INTRODUCTION TO THE FRIEDMANN AND LEMAÎTRE – TOLMAN MODELS

This is a summary of basic facts about the L–T model. For extended expositions see Refs. [10, 11]. Its metric is:

$$\mathrm{d}s^2 = \mathrm{d}t^2 - \frac{{R_{,r}}^2}{1+2E(r)}\mathrm{d}r^2 - R^2(t,r)(\mathrm{d}\vartheta^2 + \sin^2\vartheta\,\mathrm{d}\varphi^2), \tag{2.1}$$

where $E(r)$ is an arbitrary function, and $R(t,r)$ is determined by the integral of the Einstein equations:

$${R_{,t}}^2 = 2E(r) + 2M(r)/R - \tfrac{1}{3}\Lambda R^2, \tag{2.2}$$

$M(r)$ being another arbitrary function and Λ being the cosmological constant. Note that E must obey

$$2E + 1 \geq 0 \tag{2.3}$$

in order that the signature of (2.1) is the physical $(+---)$. The equality in (2.3) can occur only at special locations (at isolated values of r) called necks [11].

Equation (2.2) has the same algebraic form as one of the Friedmann equations, except that it contains arbitrary functions of r in place of arbitrary constants. The solution of (2.2) may be written as

$$t - t_B(r) = \pm \int \frac{\mathrm{d}R}{\sqrt{2E(r) + 2M(r)/R - \frac{1}{3}\Lambda R^2}}, \tag{2.4}$$

where $t_B(r)$ is one more arbitrary function called the bang time. The $+$ sign applies for an expanding region, $-$ applies for a collapsing region. Throughout this paper only expanding models will be considered.

In the case $\Lambda = 0$, the solutions of (2.2) may be written in the parametric form as follows:

(1) When $E(r) < 0$:

$$\begin{aligned} R(t,r) &= -\frac{M}{2E}(1-\cos\eta), \\ \eta - \sin\eta &= \frac{(-2E)^{3/2}}{M}\left[t - t_B(r)\right]. \end{aligned} \tag{2.5}$$

(2) When $E(r) = 0$:

$$R(t,r) = \left\{\frac{9}{2}M(r)\left[t - t_B(r)\right]^2\right\}^{1/3}. \tag{2.6}$$

(3) When $E(r) > 0$:

$$\begin{aligned} R(t,r) &= \frac{M}{2E}(\cosh\eta - 1), \\ \sinh\eta - \eta &= \frac{(2E)^{3/2}}{M}\left[t - t_B(r)\right]. \end{aligned} \tag{2.7}$$

The mass density is

$$\kappa\rho = \frac{2M_{,r}}{R^2 R_{,r}}, \qquad \kappa \stackrel{\mathrm{def}}{=} \frac{8\pi G}{c^2}. \tag{2.8}$$

The pressure is zero, so the matter (dust) particles move on geodesics.

Equations (2.1) – (2.8) are covariant with the transformation $r \to r' = f(r)$, which may be used to give one of the functions (M, E, t_B) a handpicked form, in the range where it is monotonic. In this paper, $M_{,r} > 0$ is assumed, and the following choice of r will be made

$$M = M_0 r^3, \tag{2.9}$$

where $M_0 > 0$ is an arbitrary constant. This r is still not unique – the transformations $r = Cr'$, with $C =$ constant, are still allowed, and they redefine M_0 by $M_0 = M_0'/C^3$. So, we can assume a convenient value for M_0. However, M_0 has the dimension of length and represents mass, so the choice of its value amounts to choosing a unit of mass. See Sec. X for more on this.

As seen from (2.8), the locus of $R_{,r} = 0$ is a curvature singularity ($\rho \to \infty$), unless it coincides with the locus of $M_{,r} = 0$ – but this last one is absent here because of (2.9). This singularity is called *shell crossing* because, as seen from (2.1), the geodesic distance between the r- and $(r + \mathrm{d}r)$ spheres becomes zero there. The full set of necessary and sufficient conditions for avoiding shell crossings was worked out in Ref. [12]. With the assumption $M_{,r} > 0$, and $E_{,r} > 0$ adopted further on, the necessary and sufficient condition for the absence of shell crossings is

$$\frac{\mathrm{d}t_B}{\mathrm{d}r} < 0. \tag{2.10}$$

In the case $E = 0$, $R_{,r} = 0$ implies, via (2.6) and (2.9)

$$t - t_B(r) = \tfrac{2}{3} r \frac{\mathrm{d}t_B}{\mathrm{d}r}. \tag{2.11}$$

Since $r > 0$ by assumption (2.9), and $t > t_B$ in expanding models, (2.11) has no solutions when $\mathrm{d}t_B/\mathrm{d}r < 0$.

It must be stressed that the L–T model, having zero pressure, cannot be applied to those cosmological situations, in which pressure cannot be neglected, in particular to the pre-recombination epoch. Consequently, if a shell crossing exists, but occurs before last scattering (usually

assumed to take place between 3×10^5 and 4×10^5 y after the Big Bang), then it is cosmologically irrelevant – the L–T model does not apply to those times anyway.

A past radial null geodesic is given by the equation

$$\frac{\mathrm{d}t}{\mathrm{d}r} = -\frac{R_{,r}}{\sqrt{1+2E(r)}}, \tag{2.12}$$

and its solution is denoted $t = t_{\rm ng}(r)$. The redshift $z(r)$ along $t_{\rm ng}(r)$ is given by [11, 13]:

$$\frac{1}{1+z}\ \frac{\mathrm{d}z}{\mathrm{d}r} = \left[\frac{R_{,tr}}{\sqrt{1+2E}}\right]_{\rm ng}. \tag{2.13}$$

Given $t_{\rm ng}(r)$ and $z(r)$, the luminosity distance $D_L(z)$ of a light source from the central observer is [14]

$$D_L(z) = (1+z)^2\ R|_{\rm ng}\,. \tag{2.14}$$

The Friedmann limit of (2.1) follows when $M/r^3 = M_0$, $2E/r^2 = -k$ and t_B are constant, where k is the Friedmann curvature index. Then (2.5) – (2.7) imply $R = rS(t)$,[1] and the limiting metric is

$$\mathrm{d}s^2 = \mathrm{d}t^2 - S^2(t)\left[\frac{1}{1-kr^2}\mathrm{d}r^2 + r^2(\mathrm{d}\vartheta^2 + \sin^2\vartheta\,\mathrm{d}\varphi^2)\right]. \tag{2.15}$$

Equation (2.13), using (2.12), simplifies to $(\mathrm{d}z/\mathrm{d}t)/(1+z) = S_{,t}\,/S$, which is easily integrated to give

$$1 + z = S(t_o)/S(t_e), \tag{2.16}$$

where t_o and t_e are the instants of, respectively, observation and emission of the light ray.

In the Friedmann limit, the formula for the luminosity distance can be represented as follows

$$D_L(z) = \frac{1+z}{H_0\sqrt{\Omega_k}} \times \sinh\left\{\int_0^z \frac{\sqrt{\Omega_k}\mathrm{d}z'}{\sqrt{\Omega_m(1+z')^3 + \Omega_k(1+z')^2 + \Omega_\Lambda}}\right\}, \tag{2.17}$$

where H_0 is the Hubble coefficient at t_o:

$$H_0 = S_{,t}\,/S|_{t=t_o} \tag{2.18}$$

and the three dimensionless parameters

$$(\Omega_m, \Omega_k, \Omega_\Lambda) \stackrel{\rm def}{=} \frac{1}{3{H_0}^2}\left(\frac{8\pi G\rho_0}{c^2}, -\frac{3k}{{S_0}^2}, -\Lambda\right)\Big|_{t=t_o} \tag{2.19}$$

obey $\Omega_m + \Omega_k + \Omega_\Lambda \equiv 1$ (ρ_0 is the current mean mass density in the Universe and $S_0 = S(t_o)$). This formula applies also with $\Omega_k < 0$ ($\sinh(\mathrm{i}x) \equiv \mathrm{i}\sin x$) and $\Omega_k \to 0$. In the last case (2.17) simplifies to

$$D_L(z) = \frac{1+z}{H_0}\int_0^z \frac{\mathrm{d}z'}{\sqrt{\Omega_m(1+z')^3 + \Omega_\Lambda}}, \tag{2.20}$$

where now $\Omega_m + \Omega_\Lambda \equiv 1$.

Note that the time coordinate t used here is related to the physical time τ (measured, for example, in years) by $t = c\tau$. Therefore, the Hubble parameter H_0 defined in (2.18) is related to the quantity $\mathcal{H}_0$ named "Hubble constant" in astronomical tables by

$$H_0 = \mathcal{H}_0/c. \tag{2.21}$$

III. APPARENT HORIZONS IN THE L–T AND FRIEDMANN MODELS

A general definition of an apparent horizon is given in Ref. [15]. In application to the L–T models, one deals with a simpler situation [16], [11]. An apparent horizon (AH) is the boundary of a region of spacetime, in which all bundles of null geodesics converge (have negative expansion scalar – for a model collapsing toward a final singularity) or diverge (have positive expansion scalar – for a model expanding out of a Big Bang). The first kind of AH is called the future AH, the second one – the past AH. In what follows, only the past AHs will appear and the adjective "past" will be dropped.

The AH of the central observer is a locus where R, calculated along a past-directed null geodesic given by (2.12), changes from increasing to decreasing, i.e., where

$$\frac{\mathrm{d}}{\mathrm{d}r}R(t_{\rm ng}(r), r) = 0. \tag{3.1}$$

This locus is given by [11]

$$2M/R - 1 - \tfrac{1}{3}\Lambda R^2 = 0. \tag{3.2}$$

Equation (3.2) has a solution for every value of Λ (see Appendix A). Thus, as we proceed backward in time along the central past light cone, the radius of the light cone first increases until the AH is reached, then decreases, and this happens independently of the presence and sign of Λ. The same applies to the Friedmann models [17].

From now on, $\Lambda = 0$ will be assumed for the L–T model, so the AH will be at

$$R = 2M = 2M_0 r^3. \tag{3.3}$$

In the Friedmann limit this becomes

$$S(t) = 2M_0 r^2. \tag{3.4}$$

IV. THE TILT OF THE MATTER VELOCITY VECTOR WITH RESPECT TO THE LIGHT CONE IN THE $k = 0$ FRIEDMANN MODEL

In Sections IV – VII the subcase $E = 0$ of the L–T model will be considered, and the values of its parameters

[1] A coordinate-independent condition for the Friedmann limit is $2E/M^{2/3}$ and t_B being constant. Then $R = [M(r)/M_0]^{1/3}S(t)$.

will be unrelated to reality; they will be chosen so as to achieve the best visualisation. For a radial null geodesic directed toward the center of symmetry, (2.12) implies that the components of its tangent vector field obey

$$k^t/k^r = -\,R_{,r}|_{\rm ng}\,. \tag{4.1}$$

This is a measure of the angle between the light cone and the flow lines of the cosmic medium. In the Friedmann limit, with r chosen as in (2.15), the above becomes

$$k^t/k^r\big|_{\rm F} = -\,S(t)|_{\rm ng}\,. \tag{4.2}$$

This determines the redshift via (2.16).

In the following, we will use the cosmologists' favourite Friedmann model, in which $k = 0$ and $\Lambda < 0$. In this case, with r defined as in (2.9), eq. (2.2) becomes

$$S_{,t}{}^2 = \frac{2M_0}{S} - \frac{1}{3}\Lambda S^2. \tag{4.3}$$

This has the elementary solution

$$S_\Lambda(t) = \left(-\frac{6M_0}{\Lambda}\right)^{1/3} \sinh^{2/3}\left[\frac{\sqrt{-3\Lambda}}{2}\,(t - t_{B\Lambda})\right], \tag{4.4}$$

where $t_{B\Lambda}$ is an arbitrary constant – the time coordinate of the Big Bang. For $\Lambda = 0$ the solution of (4.3) is

$$S(t) = \left(\frac{9M_0}{2}\right)^{1/3} (t - t_{B0})^{2/3}\,, \tag{4.5}$$

where t_{B0} is another constant. Figure 1 shows a comparison of $S_\Lambda(t)$ and $S(t)$. (For the sake of easier comparison, the curve (4.4) in Fig. 1 is shifted to $t_{B\Lambda} = -11$ instead of $t_{B\Lambda} = -15$ used in most other figures.)

The following should be noted:

(1) The curve $S(t)$ is concave everywhere, while $S_\Lambda(t)$ is concave up to the instant $t = t_i$, where

$$t_i - t_{B\Lambda} = \frac{1}{\sqrt{-3\Lambda}} \ln\left(\frac{\sqrt{3}+1}{\sqrt{3}-1}\right), \tag{4.6}$$

and for $t > t_i$ becomes convex. At the inflection point $t = t_i$ the accelerated expansion sets in.

(2) If $t_{B\Lambda} = t_{B0}$, then $S_\Lambda(t)$ and $S(t)$ are tangent at $t = t_{B0}$.

(3) With $t_{B\Lambda} = t_{B0}$ we have, at any $t > t_{B0}$

$$S_\Lambda(t) > S(t) \qquad \text{and} \qquad S_{\Lambda,t} > S_{,t}\,. \tag{4.7}$$

The basic measured quantity in cosmology is the Hubble parameter (2.18). Suppose, we want to compare the models (4.4) and (4.5), taking H_0 as given. Then, for H_0 being the same in both models, (2.18) implies

$$\frac{\sqrt{-3\Lambda}}{2}\,\coth\left[\frac{\sqrt{-3\Lambda}}{2}\,(t - t_{B\Lambda})\right] = \frac{1}{t - t_{B0}}. \tag{4.8}$$

Since $\coth x > 1/x$ for all $x > 0$, Eq. (4.7) implies

$$t_{B\Lambda} < t_{B0}, \tag{4.9}$$

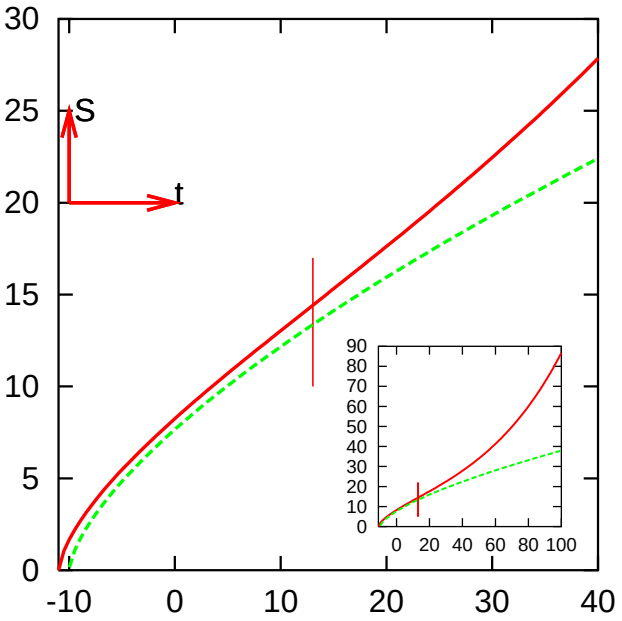

FIG. 1: A comparison of the curves (4.4) (the upper line) and (4.5) (the lower line). At the inflection point (marked by the vertical bar) the accelerated expansion in (4.4) sets in. The inset shows the same curves over a longer period of time. The parameters are $(M_0, \Lambda, t_{B0}, t_{B\Lambda}) = (1, -0.001, -10, -11)$.

i.e. the Universe is older in the model (4.4) than in (4.5).

For later reference let us note that (3.2) for the model (4.4), in the (t, R) variables, has the form

$$t = t_{B\Lambda} + \frac{2}{\sqrt{-3\Lambda}}\,\ln\left(\frac{1 + \sqrt{-\Lambda/3}R}{\sqrt{1 + \Lambda R^2/3}}\right). \tag{4.10}$$

V. THE ACCELERATED EXPANSION

With the $S(t)$ of (4.5) the radial null geodesic equation for the metric (2.15) can be integrated:

$$(t - t_{B0})^{1/3} = (t_o - t_{B0})^{1/3} - (M_0/6)^{1/3} r, \tag{5.1}$$

where (t, r) are the coordinates of the point on the geodesic and $t = t_o$ is the instant of observation, at which $r = 0$. Figure 2 shows this geodesic, compared with the null geodesic corresponding to (4.4), taking (4.9) into account. With $\Lambda < 0$, the angle α_2 between the geodesic and the flow lines of matter (which are the vertical straight lines) is everywhere smaller than the corresponding angle α_1 for $\Lambda = 0$, because of (4.7) and (4.2).

As we proceed back in time toward the Big Bang, more and more particles of the cosmic matter are encompassed by the light cone. This is seen from (5.1), where $r(t)$ is

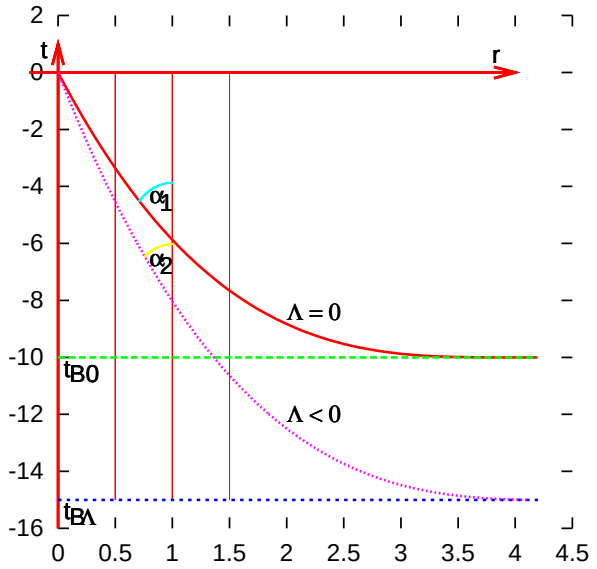

FIG. 2: The past null geodesic $t(r)$ for the metric (2.15) with $k = 0 = \Lambda$ (upper curve) and with $k = 0 > \Lambda$ (lower curve). The vertical straight lines are world lines of the cosmic medium. We have $\alpha_2 < \alpha_1$ everywhere. The observer is at $(t, r) = (0, 0)$; $t_{B\Lambda} = -15$, other parameters are the same as in Fig. 1. This graph does not faithfully show the radius of the intersection of the light cone with a hypersurface of constant t; for that see Fig. 3.

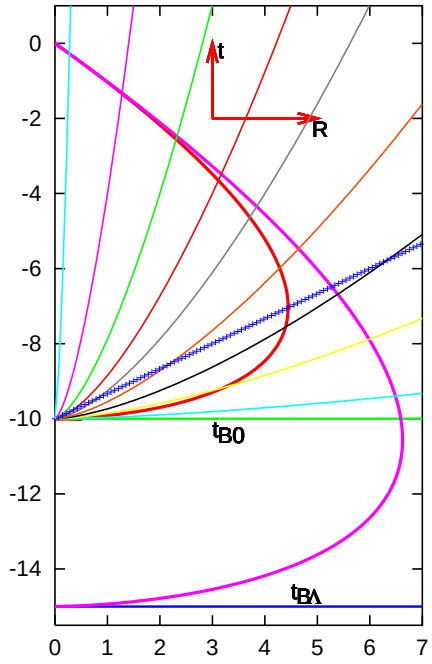

FIG. 3: The geodesic radius $R = rS(t(r))$ of the null cones from Fig. 2 as a function of t. The curves fanning out of the point $(t, R) = (-10, 0)$ are images of the vertical straight lines of Fig. 2. Each one of them has a different value of r. Note the maximal value of r, beyond which the radius of the cone decreases toward the Big Bang – this is where the light cone intersects the past apparent horizon of (4.5), shown as the jagged straight line.

decreasing in $t \in [t_{B0}, t_o]$. However, $r(t_{B0})$ is finite,[2]

$$r(t_{B0}) = [6(t_o - t_{B0})/M_0]^{1/3}\,, \tag{5.2}$$

i.e. the mass within the light cone is finite at the Big Bang (but $r(t_{B0})$ increases as t_o increases.) The same is true for the S_Λ of (4.4): because of (4.7) we have

$$r(t_{B\Lambda}) = \int_{t_{B\Lambda}}^{t_o} \frac{\mathrm{d}t}{S_\Lambda} < \int_{t_{B\Lambda}}^{t_o} \frac{\mathrm{d}t}{S} < \infty. \tag{5.3}$$

Figure 2 does not correctly display the spatial radius of the light cones. It gives the illusion that the radius becomes ever larger toward the Big Bang. This is not the case. With $k = 0$, the invariant radius of the light cone at time t is $R \overset{\text{def}}{=} rS(t(r))$, where $t(r)$ is the function implied by (5.1) or its $\Lambda < 0$ counterpart. Figure 3 shows the graphs of R against t along the light cones of the models (4.4) and (4.5). As is seen, when we proceed toward the past, the radius of the light cone increases at first, but acquires a maximum at a certain instant and then decreases to zero as the Big Bang is approached.[3]

The maximum is at the intersection of the light cone with the past apparent horizon (AH) [11, 16]. The general equation of AH, (3.4), for the model (4.5) reduces to $t = t_B + (2/3)R$, this line is also shown in Fig. 3.

Figure 3 also shows the flow lines of matter for the model (4.5) in the (t, R) variables. They are all convex because the functions $R(t)$ that they represent all have $R_{,tt} < 0$ (decelerated expansion).

The inflection points of the flow lines for the model (4.4), where the accelerated expansion begins, with the parameter values used in Fig. 3, lie far to the future of the observer position $(t, R) = (0, 0)$. Therefore, for comparison, Fig. 4 shows the corresponding picture for the model (4.4), with the parameter values suitably adapted. It also shows the AH for this model, calculated from (4.10).

The observer does not know, which spacetime he/she is in, and only collects light signals from the light cone. For the purpose of comparing the observations carried out in the background of the model of (4.4) with those carried out in the background of (4.5), we have to imagine the light cone of (4.4) being mapped into the light cone of (4.5) in such a way that the identity of the cosmic particles and the angle α_2 (which is a measure of the velocity of expansion) are preserved. To preserve the

[2] The matter particle that leaves the Big Bang at $r(t_{B0})$ is at the particle horizon [18], [11] at $t = t_o$.

[3] The past light cones of the L–T models with $\Lambda = 0$ have the same property. It is this feature that was mistaken for a "pathology" and named "critical point" in Ref. [9].

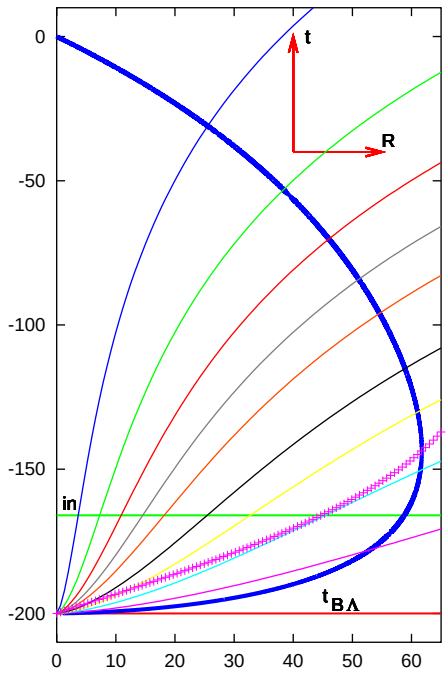

FIG. 4: The geodesic radius $R = rS(t(r))$ of the null cone corresponding to (4.4) as a function of t, and a collection of world lines of the cosmic medium corresponding to different values of r. The horizontal line marked "in" is where all the world lines have their inflection points. The jagged curve is the AH given by (4.10). The values of the parameters are $(M_0, \Lambda, t_{B\Lambda}) = (1, -0.0005, -200)$.

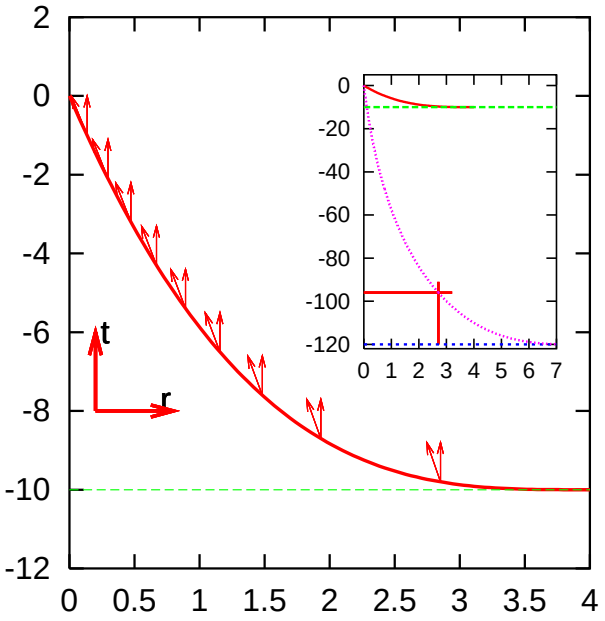

FIG. 5: When the observer at $(t, r) = (0, 0)$ interprets the redshift observations against the background of the model (4.4), the flow lines of cosmic matter are tilted toward the light cone by more than was the case in (4.5). This excess tilt is a measure of the 'accelerated expansion'. The horizontal line at the bottom marks the time of the Big Bang for (4.5). The value of $t_{B\Lambda}$ is -120; other parameters are the same as in Fig. 1. The inset shows Fig. 2 with $t_{B\Lambda}$ changed from -15 to -120. The crossing straight lines in the inset mark the inflection point, where accelerated expansion begins.

identity means to move each point of the lower curve of Fig. 2 into the upper curve along a vertical straight line.

Figure 5 shows the result of such a mapping. The $t_{B\Lambda}$ in it is -120, so, by (4.6), the accelerated expansion begins at $(t, r) \approx (-96.0, 2.708)$. With (4.5), all the flow lines have vertical tangents, as in Fig. 2. With (4.4), the flow lines tilt away from the vertical, more and more toward the light cone as t increases. The observer concludes that in the model given by (4.4) the expansion rate of the Universe increases with time.

VI. EXPLAINING AWAY THE "ACCELERATED EXPANSION" BY A NONSIMULTANEOUS BIG BANG

It is shown below that the function $(k^t/k^r)(r)$ along the past light cone of the observer implied by (4.4) can be obtained using the $E = 0$ L–T model. In order to calculate it, the corresponding null geodesic equation for (2.15) with (4.4) is first solved:

$$\frac{\mathrm{d}t}{\mathrm{d}r} = -\left(\frac{6M_0}{-\Lambda}\right)^{1/3} \sinh^{2/3}\left[\frac{\sqrt{-3\Lambda}}{2}\,(t - t_{B\Lambda})\right]. \quad (6.1)$$

The solution (found numerically and shown in Fig. 2) will be denoted $t = t_F(r)$. When it is substituted in (4.4), it determines $(k^t/k^r)_F(r)$ via (4.2).

The corresponding k^t/k^r in the L–T model (2.6) is found from (2.12), which, with r chosen as in (2.9), reads

$$\frac{\mathrm{d}t}{\mathrm{d}r} = \left(\frac{9M_0}{2}\right)^{1/3} \Big\{ -[t - t_B(r)]^{2/3} + \frac{2}{3}\, r\,[t - t_B(r)]^{-1/3}\, t_{B,r} \Big\}. \quad (6.2)$$

The solution of (6.2) will be denoted $t = t_{LT}(r)$.

The same function $(k^t/k^r)(r)$ along the past light cone in both models will thus follow when

$$\left(\frac{\mathrm{d}t}{\mathrm{d}r}\right)_F = \left(\frac{\mathrm{d}t}{\mathrm{d}r}\right)_{LT}. \quad (6.3)$$

This means that t_F and t_{LT} will coincide at the observer's position when $t_F = t_{LT}$ everywhere on the cone. Consequently, $t_F(r)$ must be found from (6.1), then substituted for t in (6.2). The result can be written as

$$\frac{\mathrm{d}t_B}{\mathrm{d}r} = \frac{3}{2r}\left\{ \left(\frac{2}{9M_0}\right)^{1/3} [t_F(r) - t_B(r)]^{1/3}\, \frac{\mathrm{d}t_F}{\mathrm{d}r} + t_F(r) - t_B(r) \right\}, \quad (6.4)$$

where $\mathrm{d}t_F/\mathrm{d}r$ is given by (6.1). A necessary condition for $t_{B,r}$ to be finite at $r = 0$ is that the expression in braces

tends to zero when $r \to 0$. This will happen if

$$\lim_{r\to 0} \frac{\sinh\left\{\frac{\sqrt{-3\Lambda}}{2}\left[t_F(r) - t_{B\Lambda}\right]\right\}}{\frac{\sqrt{-3\Lambda}}{2}\left[t_F(r) - t_B(r)\right]} = 1. \qquad (6.5)$$

This determines the value of $t_B(0)$:

$$\begin{aligned} t_B(0) &= t_F(0) - \frac{2}{\sqrt{-3\Lambda}} \sinh\left\{\frac{\sqrt{-3\Lambda}}{2}\left[t_F(0) - t_{B\Lambda}\right]\right\} \\ &< t_{B\Lambda}. \end{aligned} \qquad (6.6)$$

Note that $[t_F(0) - t_B(0)]$ increases when $|\Lambda|$ increases. With (6.6) fulfilled, (6.4) implies

$$\begin{aligned} \lim_{r\to 0} \frac{\mathrm{d}t_B}{\mathrm{d}r} &= \frac{1}{2}\left(\frac{6M_0}{-\Lambda}\right)^{1/3} \\ &\times \left\{\cosh\left[\frac{\sqrt{-3\Lambda}}{2}\left(t_F(0) - t_{B\Lambda}\right)\right] - 1\right\} \\ &\times \sinh^{2/3}\left[\frac{\sqrt{-3\Lambda}}{2}\left(t_F(0) - t_{B\Lambda}\right)\right] > 0. \end{aligned} \qquad (6.7)$$

This implies $\lim_{r\to 0} \rho_{,r} > 0$ for the ρ of (2.8), which relates in two ways to problems considered in the literature:

1. The property $\rho_{,r} \neq 0$ at the center was called "weak singularity" [9]. However, this is not a singularity in the sense of any definition used in relativity [19].

2. When $\rho_{,r} > 0$ at the center, the density increases with distance from the center, i.e. there is a void around the center. Some authors claimed that the presence of this void is a necessary feature of any L–T model used to mimic accelerated expansion. The model considered in our Secs. VIII – XVIII is a counterexample to this claim.

Figure 6 shows the graph of $t_B(r)$ calculated from (6.4), the corresponding past light cone for the central observer, and the $\Lambda < 0$ past light cone from Fig. 2, included for comparison. The two light cones coincide up to numerical errors $\Delta t \approx 0.015$. Assuming that $-t_{B\Lambda} = 15$ represents the age of the Universe $T = 13.819 \times 10^9$ y [3], this error translates to $\Delta t = 10^{-3}T = 1.38 \times 10^7$ y.

Since in all the models comoving coordinates were used, the flow lines of matter are vertical straight lines in every case. Therefore, identical light cones for the two models mean identical functions k^t/k^r for both.

The inset in Fig. 6 shows the shell crossing (given by (2.11)), which is in this case inevitable, since $t_B(r)$ is increasing all the way. (At the scale of the main figure, the shell crossing would coincide with the Big Bang.)

Since the example discussed up to now was not meant to reflect any real measurements done in astronomy, the question whether the shell crossings pose a serious problem is irrelevant. But, for the sake of completeness, let us note the following. The biggest time-difference between the shell crossing and the Big Bang is 0.0885 time units used in the figure, while the time-difference at the right margin is 0.0354. This translates to 8.15×10^7 y and 3.26×10^7 y, respectively. This is to be compared with

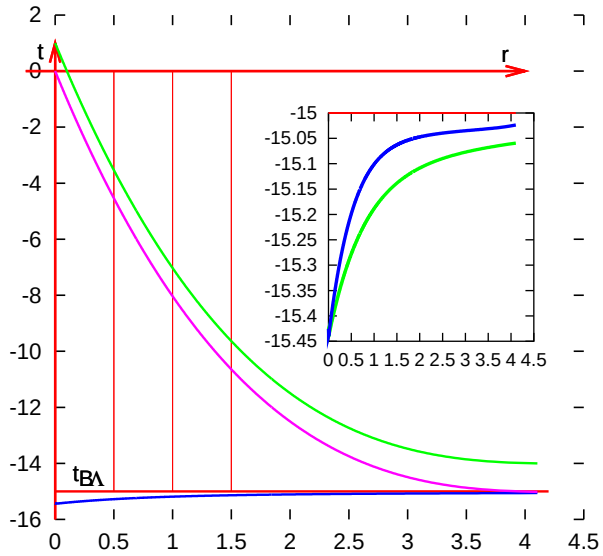

FIG. 6: **Lowest curve:** The function $t_B(r)$ defined by (6.4) and (6.1). **Middle curve:** The L–T light cone calculated from (6.2) with $t_B(r)$ as in the lowest curve. **Upper curve:** The $\Lambda < 0$ light cone from Fig. 2, shifted by $\Delta t = 1$ upwards, included for comparison. The inset shows a closeup view of the time interval between the shell crossing (upper curve) and the Big Bang (lower curve).

$t - t_B \approx 3.5 \times 10^5$ years for the recombination epoch – so, clearly, this is not a realistic model of our Universe.

It is interesting to transform Fig. 6 to the variables (t, R), in analogy to Fig. 4. It is shown in Fig. 7. Now the Big Bang is no longer a single point, but a segment of the t-axis. This reflects the fact that the Big Bang occurs at different times for different flow lines. The flow lines no longer have a common origin, and they intersect in the vicinity of their origins. The intersections are images of the shell crossings, shown in closeup view in Fig. 8.

The light cone in Fig. 7 does not extend to the $R = 0$ line because of numerical errors. They cause that the light cone in Fig. 6 ends at $r \approx 4$, where it has not yet met the Big Bang set, so R is not yet zero there, and the gap is magnified in the transformation. For the same reason, the two light cones from Fig. 6 coincide with a smaller precision after the transformation – the image of the $\Lambda < 0$ Friedmann cone is seen in the vicinity of the maximal radius in Fig. 7.

VII. COMMENTS

Since solving (6.1) only requires calculating an integral of a function of r which is evidently integrable, the solution exists for every $t_{B\Lambda}$. The same is true for (6.2): the $t_B(r)$ determined by it exists for every $t_F(r)$. However, the solution of (6.1) defines *a single light cone* of (2.15). *The same* L–T model will not mimic all light rays in (4.4) reaching a given observer. The time evolution of the L–

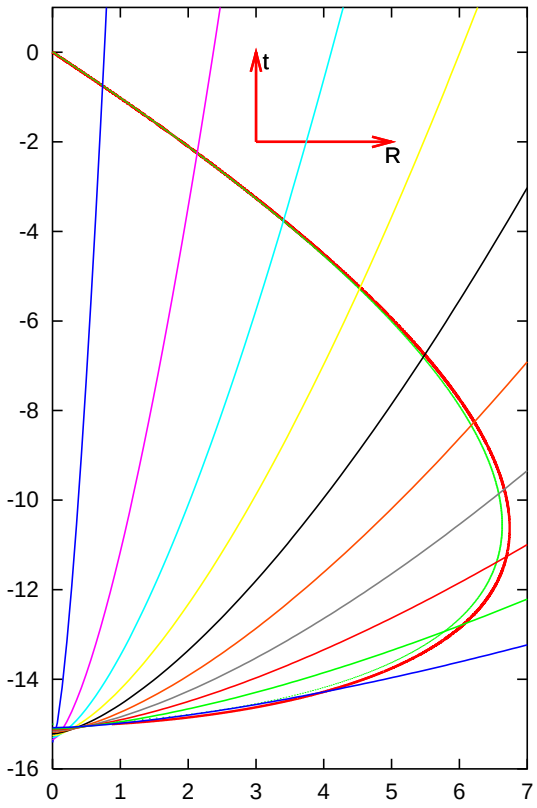

FIG. 7: The geodesic radius $R(t(r))$ of the null cone defined by (6.2) and (6.4) as a function of t, and a collection of flow lines of the cosmic medium corresponding to different values of r. The Big Bang is now a finite segment of the t-axis. Note the intersections of the flow lines in the vicinity of their origins – they are images of shell crossings. A closeup view of the shell crossings is shown in Fig. 8. The second curve seen in the neighbourhood of maximal R is a copy of the light cone from Fig. 4. The two cones do not perfectly coincide in consequence of numerical errors.

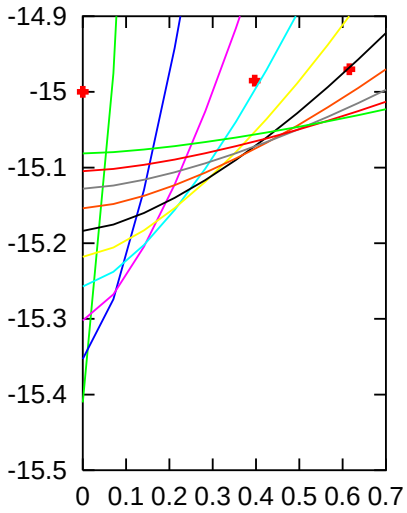

FIG. 8: A closeup view of the region of shell crossings in Fig. 7. The crosses mark the $\Lambda < 0$ Friedmann null cone.

T model with $\Lambda = 0$ is different from that of the ΛCDM model, and the two can be distinguished by observations that are sensitive to the dynamics of the Universe, and not just to a momentary "snapshot". Examples of effects that depend on the time-evolution are redshift drift [8] and non-repeatability of light paths [20–22].

The function $t_B(r)$ in Fig. 6 is increasing, and $t_B(r) < t_{B\Lambda}$ at all r. To get an understanding why this is so, let us observe the following. The L–T model of (2.6) expands by the same law as the $k = 0$ Friedmann model with $\Lambda = 0$. Because of (4.7) the function $(k^t/k^r)_F = -S_\Lambda(t)$ decreases faster with t than $(k^t/k^r)_{LT} = -R_{,r}$ at $r = 0$. Hence, in order to *slow down* to the same rate of decrease as $(-S_\Lambda)$, the function $(-R_{,r})$ needs more time, so $t_B(0)$ must precede $t_{B\Lambda}$. With the age of the Universe $(t(r) - t_{B\Lambda})$ decreasing along the past light cone, $t_B - t_{B\Lambda}$ must also decrease, so $t_B(r)$ must be increasing. In order to obtain $t_B(r) > t_{B\Lambda}$, one needs to consider a quantity that either decreases slower or increases faster in the ΛCDM model than in L–T.

Since just one of the two arbitrary functions in the L–T model suffices to mimic accelerated expansion, it is natural to suppose that with both functions, $E(r)$ and $t_B(r)$, being arbitrary, the L–T model can be adapted to two sets of observations. In Ref. [7] it was explicitly demonstrated that this is indeed possible for the pairs (angular diameter distance – mass density in the redshift space) and (angular diameter distance – expansion rate).

Note how eq. (6.2) displays an instability of the Friedmann model with respect to the L–T perturbation.[4] In the Friedmann limit, we have $t_{B,r} = 0$, so $\lim_{t\to t_B} \mathrm{d}t/\mathrm{d}r = 0$, i.e., in the comoving coordinates, the tangent to each null geodesic becomes horizontal at the Big Bang. However, in the L–T model, at every $r > 0$ where $t_{B,r} \neq 0$, we have $\lim_{t\to t_B} |\mathrm{d}t/\mathrm{d}r| = \infty$, i.e. the tangent to the null geodesic is vertical. The only exceptions are points in which $t_{B,r} = 0$, where the said tangent is horizontal even in L–T. Thus, since in our L–T model the current observer's light cone is the same as in a Friedmann model, this light cone must be horizontal at $t = t_B$. This means that the observer who carried out this construction must live in a special epoch: that, in which her past light cone intersects with the extremum/inflection of the Big Bang set. This should not be disturbing from the point of view of astrophysics, for the following reasons:

1. The dust models do not apply just after the Big Bang – the pressure cannot be assumed zero at those early times. They begin to apply no earlier than after last scattering. Considering the light cones up to the Big

[4] This was first observed by Szekeres [23], and discussed in more detail by Hellaby and Lake [24], see also Ref. [11].

Bang was a geometric exercise, whose results are not to be taken as implications for our physical Universe.

2. Light from objects that might have existed before last scattering is not observed. Hence, we have no observational clues as to the state of the Universe prior to that epoch. (The situation might improve when neutrinos and gravitational waves from the early Universe can be registered, but this will happen in the future, perhaps distant future.) Also, there is a long gap between the highest-redshift objects observed so far ($z \approx 10$)[5] and the last scattering epoch ($z \approx 1089$ [26]); we have no direct information from that segment of our past light cone. Consequently, the attempt to reconstruct our whole past light cone up to its contact with the Big Bang is excessively ambitious – the result is not observationally testable.

3. For simplicity, the adequacy of the ΛCDM model was not discussed here, and the values of its parameters were taken for granted. However, in order to test the L–T model against observations in earnest, one would have to use it in the analysis of observational data from the beginning to the end. The L–T model should be adapted directly to the observational data, and not to the parameters of the best-fit Friedmann model. Such an analysis still remains to be done.

The peculiar properties of the L–T light cone will be present also in the model discussed further on, see eqs. (11.2) and (11.4).

The discussion up to this place was presented for illustrative purposes. It is related to astrophysics indirectly, but is free from numerical complications. From the next section on, a more realistic example will be described.

VIII. DUPLICATING THE LUMINOSITY DISTANCE – REDSHIFT RELATION USING THE L–T MODEL WITH $\Lambda = 0$

Now it will be shown how the luminosity distance – redshift relation of the ΛCDM model (our eq. (2.20)) can be duplicated using the L–T model with $\Lambda = 0$. The reasoning below was inspired by Iguchi et al. [6].

To duplicate (2.20) using the $\Lambda = 0$ L–T model means, in view of (2.14) and (2.20), to require that

$$R(t_{\rm ng}(r), r) = \frac{1}{H_0(1+z)} \int_0^z \frac{{\rm d}z'}{\sqrt{\Omega_m(1+z')^3 + \Omega_\Lambda}} \tag{8.1}$$

holds along the past light cone of the central observer, where H_0, Ω_m and Ω_Λ have the values determined by current observations, $t_{\rm ng}(r)$ is the function determined by (2.12) and $z(r)$ is determined by (2.13). Let

$$\mathcal{D}(z) \stackrel{\rm def}{=} \int_0^z \frac{{\rm d}z'}{\sqrt{\Omega_m(1+z')^3 + \Omega_\Lambda}}. \tag{8.2}$$

Note that $\mathcal{D}(0) = 0$, $\mathcal{D}(z) > 0$ at all $z > 0$ and $\mathcal{D}_{,z} > 0$ at all $z \geq 0$, but $\lim_{z\to\infty} \mathcal{D}(z)$ is finite, since, for $\Omega_\Lambda > 0$ (as is the case in the ΛCDM model) at all z we have

$$\begin{aligned} \mathcal{D}(z) &< \int_0^z \frac{{\rm d}z'}{\sqrt{\Omega_m(1+z')^3}} \\ &= \frac{2}{\sqrt{\Omega_m}} \left(1 - \frac{1}{\sqrt{1+z}}\right) < \frac{2}{\sqrt{\Omega_m}} < \infty. \end{aligned} \tag{8.3}$$

Unlike in the RW models, light emitted at the Big Bang of an L–T model and reaching an observer is in general infinitely blueshifted, i.e. $z_{\rm BB} = -1$, except when $t_{B,r} = 0$ at the emission point [23], [24], [11] – then it may have infinite redshift. As follows from (8.1) and (8.3), at the Big Bang, where $R = 0$, $z \to \infty$ must hold. This implies that, just like in the previous example in Sec. VII, $t_{B,r} \to 0$ at the emission point of the ray (8.1) should hold. Note also, from (8.1) and (8.3) again, that at the Big Bang, where $z \to \infty$, the following is true

$$\lim_{z\to\infty} \{R_{\rm ng}(1+z)\} = C_0 < \infty. \tag{8.4}$$

IX. LOCATING THE APPARENT HORIZON

Recall: at the AH $({\rm d}/{\rm d}r)\, R|_{\rm ng} = 0$ [16], [11]. Thus, differentiating (8.1) by r, one obtains

$$\left(A_1 \frac{{\rm d}z}{{\rm d}r}\right)_{\rm AH} = 0, \tag{9.1}$$

where

$$A_1 \stackrel{\rm def}{=} \mathcal{D} - \frac{1+z}{\sqrt{\Omega_m(1+z)^3 + \Omega_\Lambda}}. \tag{9.2}$$

Suppose, for a moment, that ${\rm d}z/{\rm d}r|_{\rm AH} = 0$. In consequence of (2.13), this would mean $R_{,tr}|_{\rm AH} = 0$. It is shown in Appendix B that this equation forces a relation between M, E and t_B, thus reducing the number of arbitrary functions to 2. So, $R_{,tr}|_{\rm AH}$ is zero only in those special cases,[6] while the general conclusion from (9.1) is

$$A_1|_{\rm AH} = 0. \tag{9.3}$$

Note that this equation does not refer to the L–T model.

With Ω_m and Ω_Λ given, the equation $A_1 = 0$ can be solved for z. Using the values $(\Omega_m, \Omega_\Lambda) = (0.32, 0.68)$ as in Ref. [3], Fig. 9 shows that $z \approx 1.583$ on the AH.

The equation of the AH, (3.3), may be written, using (8.1), (8.2) and (2.9), also as

$$r_{\rm AH} = \left[\frac{\mathcal{D}}{2M_0 H_0 (1+z)}\right]^{1/3}_{\rm AH}, \tag{9.4}$$

[5] For a somewhat outdated summary on the objects with highest redshifts see Ref. [25].

[6] The remark in Ref. [6], made after their (3.1), which implies that the locus of $R_{,tr} = 0$ coincides with $R = 2M$, is thus incorrect.

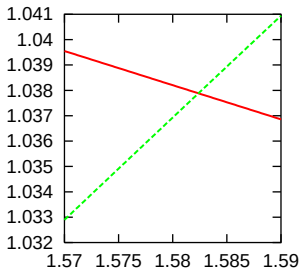

FIG. 9: Graphical solution of the equation $A_1 = 0$ with A_1 given by (9.2) and $(\Omega_m, \Omega_\Lambda) = (0.32, 0.68)$, as in Ref. [3]. The increasing function is $\mathcal{D}(z)$, the decreasing function is $(1+z)/\sqrt{\Omega_m(1+z)^3 + \Omega_\Lambda}$. The intersection of the curves is at the apparent horizon, where $z \approx 1.583$, $\mathcal{D} \approx 1.038$.

In what follows, it will be useful to define one more quantity that vanishes on the AH, in consequence of (9.4):

$$A_2 \stackrel{\text{def}}{=} \sqrt{\frac{2M_0 H_0 r^3 (1+z)}{\mathcal{D}}} - 1. \tag{9.5}$$

The equation of the AH can be written in yet another form. For the case $E > 0$, from (2.5) and (3.3), we have

$$(t - t_B)_{\text{AH}} = \tag{9.6}$$
$$\left\{ \frac{M}{(2E)^{3/2}} \left[\sqrt{\mathcal{Y}^2 - 1} - \ln\left(\mathcal{Y} + \sqrt{\mathcal{Y}^2 - 1} \right) \right] \right\}_{\text{AH}},$$

where

$$\mathcal{Y} \stackrel{\text{def}}{=} 1 + 4E. \tag{9.7}$$

For $2E/r^2 = -k =$ constant (9.6) becomes

$$(t - t_B)_{\text{AH}} = \frac{M_0}{(-k)^{3/2}} \left\{ \sqrt{(1 - 2kr^2)^2 - 1} \right.$$
$$\left. - \ln\left[1 - 2kr^2 + \sqrt{(1 - 2kr^2)^2 - 1} \right] \right\}_{\text{AH}}. \tag{9.8}$$

X. THE NUMERICAL UNITS

The following values are assumed here

$$(\Omega_m, \Omega_\Lambda, H_0, M_0) = (0.32, 0.68, 6.71, 1) \tag{10.1}$$

the first two after Ref. [3]. The H_0 is 1/10 of the observationally determined value of the Hubble constant [3]

$$\mathcal{H}_0 = cH_0 = 67.1 \text{ km/(s} \times \text{Mpc)}. \tag{10.2}$$

It follows that H_0 is measured in 1/Mpc. Consequently, choosing a value for H_0 amounts to defining a numerical length unit (call it NLU), which, with (10.1), obeys

$$H_0 = \frac{67.1}{3 \times 10^5} \frac{\text{(km/s)/Mpc}}{\text{(km/s)}} = 6.71 \frac{1}{\text{NLU}}. \tag{10.3}$$

From here

$$1 \text{ NLU} = 3 \times 10^4 \text{ Mpc}. \tag{10.4}$$

With Ω_Λ and H_0 given by (10.1) we obtain from (2.19)

$$-\Lambda = 3\Omega_\Lambda {H_0}^2 = 91.849164(\text{NLU})^{-2}. \tag{10.5}$$

Since our time coordinate is $t = c\tau$, where τ is measured in time units, t is measured in length units. So it is natural to take the NLU defined in (10.4) also as the numerical time unit (NTU). We take the following approximate values for the conversion factors [27]:

$$\begin{aligned} 1 \text{ pc} &= 3.086 \times 10^{13} \text{ km}, \\ 1 \text{ y} &= 3.156 \times 10^7 \text{ s}. \end{aligned} \tag{10.6}$$

The following relations result, using (10.4):

$$\begin{aligned} &1 \text{ NTU} = 1 \text{ NLU} = 3 \times 10^4 \text{ Mpc} \\ &= 9.26 \times 10^{23} \text{ km} = 9.8 \times 10^{10} \text{ y}. \end{aligned} \tag{10.7}$$

Using this in (10.5) we get

$$-\Lambda = 1.02 \times 10^{-7} \text{ (Mpc)}^{-2}. \tag{10.8}$$

Finally, for the age of the Universe [3]

$$T = 13.819 \times 10^9 \text{ y} \tag{10.9}$$

we obtain

$$T = \frac{13.819 \times 10^9}{9.8 \times 10^{10}} \text{ NTU} = 0.141 \text{ NTU}. \tag{10.10}$$

The values (10.5) and (10.10) will be used for the model (4.4), with $t_{B\Lambda} = -T$.

As already mentioned below (2.9), M_0 represents mass, but has the dimension of length ($M_0 = Gm_0/c^2$, where m_0 is measured in mass units). The choice $M_0 = 1$ NLU made in (10.1) simplifies all computations. The associated mass unit $M_0 c^2/G \approx 10^{57}$ kg will not appear in any other way than via M_0.

XI. THE L–T MODEL WITH $2E = -kr^2$ THAT DUPLICATES THE $D_L(z)$ OF (2.20)

The functional shape of E might be determined by tying it to an additional observable quantity, as was done in Ref. [7]. However, then the equations defining t_B and E become coupled, and numerical handling becomes instantly necessary. To keep things transparent, we will rather follow the approach of Ref. [6], and take

$$2E = -kr^2, \tag{11.1}$$

where $k < 0$ is an arbitrary constant. This E is the same as in the $k < 0$ Friedmann model. The M will be chosen as in (2.9). From (2.10) we have on the light cone

$$\frac{\mathrm{d}t}{\mathrm{d}r} = -\frac{R_{,r}}{\sqrt{1 - kr^2}}, \tag{11.2}$$

where the general formula for $R_{,r}$ is ([11], eq. (18.104))

$$R_{,r} = \left(\frac{M_{,r}}{M} - \frac{E_{,r}}{E}\right) R + \left[\left(\frac{3}{2}\frac{E_{,r}}{E} - \frac{M_{,r}}{M}\right)(t - t_B) - t_{B,r}\right] R_{,t}\,. \quad (11.3)$$

Using (11.1), (2.2) and (2.9) this simplifies to

$$R_{,r} = \frac{R}{r} - r t_{B,r}\sqrt{\frac{2M_0 r}{R} - k}. \quad (11.4)$$

Equation (11.4) substituted in (11.2) leads to the same conclusions about the L–T light cone that were formulated in paragraph 4 of Sec. VII.

With (11.1), eqs. (2.7) become

$$\cosh\eta = 1 - \frac{kR}{M_0 r}, \quad (11.5)$$

$$t - t_B = \frac{M_0}{(-k)^{3/2}}(\sinh\eta - \eta). \quad (11.6)$$

Equations (11.5) – (11.6) will now be taken along a null geodesic, i.e. the t in (11.6) will be the $t(r)$ defined by (11.2), while the R in (11.5) will be the $R_{\rm ng}$ from (8.1). We thus have from (11.6)

$$\frac{\mathrm{d}t}{\mathrm{d}r} - \frac{\mathrm{d}t_B}{\mathrm{d}r} = \frac{R}{\sqrt{-kr}}\left.\frac{\mathrm{d}\eta}{\mathrm{d}r}\right|_{\rm ng}, \quad (11.7)$$

where, from (11.5)

$$\left.\frac{\mathrm{d}\eta}{\mathrm{d}r}\right|_{\rm ng} = -\frac{kr}{\sqrt{k^2 {R_{\rm ng}}^2 - 2kM_0 r R_{\rm ng}}}\left(\frac{R_{\rm ng}}{r}\right)_{,r}. \quad (11.8)$$

Substituting for $\mathrm{d}t/\mathrm{d}r$ from (11.2) and (11.4), and for $R_{\rm ng}$ from (8.1), then using (9.2) and (9.5) as the definitions of A_1 and A_2, we obtain from (11.7)

$$B_2\left[\frac{\mathcal{D}}{H_0 r(1+z)} - \sqrt{(A_2+1)^2 - kr^2}\frac{\mathrm{d}t_B}{\mathrm{d}r}\right] = \frac{A_1\sqrt{1-kr^2}}{H_0(1+z)^2}\frac{\mathrm{d}z}{\mathrm{d}r}, \quad (11.9)$$

where

$$B_2 \stackrel{\rm def}{=} \sqrt{(A_2+1)^2 - kr^2} - \sqrt{1-kr^2}. \quad (11.10)$$

Note that at the AH, where $A_1 = A_2 = B_2 = 0$, (11.9) becomes $0 = 0$, so expressions of the form $0/0$ will be present when integrating (11.9) through the AH.

From (2.13), using (11.4) and (2.2), we obtain

$$\frac{\mathrm{d}z}{\mathrm{d}r} = \frac{1+z}{r\sqrt{1-kr^2}}\left[\sqrt{(A_2+1)^2 - kr^2} + \frac{H_0 r(1+z)\,(A_2+1)^2}{2\mathcal{D}}\frac{\mathrm{d}t_B}{\mathrm{d}r}\right]. \quad (11.11)$$

Eliminating $\mathrm{d}t_B/\mathrm{d}r$ between (11.9) and (11.11) we get

$$\frac{\mathrm{d}z}{\mathrm{d}r} = \frac{B_2(1+z)}{B_3 r\sqrt{1-kr^2}}\left[\frac{3}{2} - \frac{kr^2}{(A_2+1)^2}\right], \quad (11.12)$$

where

$$B_3 \stackrel{\rm def}{=} \frac{A_1}{2\mathcal{D}} + B_2\frac{\sqrt{(A_2+1)^2 - kr^2}}{(A_2+1)^2}. \quad (11.13)$$

Using this in (11.11) we get

$$\frac{\mathrm{d}t_B}{\mathrm{d}r} = \frac{1}{H_0 r(1+z)B_3\sqrt{(A_2+1)^2 - kr^2}} \times \left\{\mathcal{D}B_3 - A_1\left[\frac{3}{2} - \frac{kr^2}{(A_2+1)^2}\right]\right\}. \quad (11.14)$$

In some of the numerical calculations, it will be more convenient to find $r(z)$ rather than $z(r)$, and for this purpose (11.12) will be used in the form

$$\frac{\mathrm{d}r}{\mathrm{d}z} = \frac{B_3 r\sqrt{1-kr^2}}{B_2(1+z)\left[\frac{3}{2} - \frac{kr^2}{(A_2+1)^2}\right]}. \quad (11.15)$$

XII. THE LIMITS OF (11.12) AND (11.14) AT $r \to r_{\rm AH}$

At the AH, where $A_1 = A_2 = 0$, we also have $B_2 = B_3 = 0$. Consequently, in order to carry the integration through the AH in (11.12) and (11.14), the expression B_2/B_3 that becomes $0/0$ there must be handled with care. This had already been noticed in Refs. [19] and [7], and Refs. [7] and [28] demonstrated two different solutions of this problem: in Ref. [7] an interpolating polynomial, and in Ref. [28] a Taylor expansion in $(z - z_{\rm AH})$ were used in place of the numerically calculated functions in the neighborhood of the AH. In the case considered here, the limit of B_2/B_3 at the AH can be explicitly calculated, as shown below.

From (11.12) and (11.13) we obtain

$$\lim_{r\to r_{\rm AH}}\frac{\mathrm{d}z}{\mathrm{d}r} = \lim_{r\to r_{\rm AH}}\frac{(1+z)\left(3/2 - kr^2\right)}{r\sqrt{1-kr^2}\left(\frac{A_1}{2\mathcal{D}B_2} + \sqrt{1-kr^2}\right)}. \quad (12.1)$$

A simple calculation shows that

$$\lim_{r\to r_{\rm AH}}\frac{A_1}{B_2} = \lim_{r\to r_{\rm AH}}\left(\sqrt{1-kr^2}\frac{A_1}{A_2}\right). \quad (12.2)$$

Applying the de l'Hôpital rule an making use of (9.2) and of the fact that $A_1 = 0$ on the AH, we find

$$\lim_{r\to r_{\rm AH}}\frac{A_1}{A_2} = \lim_{r\to r_{\rm AH}}\left(\Omega_m r\mathcal{D}^3\frac{\mathrm{d}z}{\mathrm{d}r}\right). \quad (12.3)$$

Let the following new symbol be introduced

$$\mathcal{G} \stackrel{\text{def}}{=} \lim_{r\to r_{\rm AH}} \Big[\big(1-kr^2\big)^2 + \big(1-kr^2\big)\big(3-2kr^2\big)\,\Omega_m\mathcal{D}^2(1+z)\Big]^{1/2}. \tag{12.4}$$

Substituting (12.3) and (12.2) in (12.1) and solving for $\lim_{r\to r_{\rm AH}} \mathrm{d}z/\mathrm{d}r$ we obtain

$$\lim_{r\to r_{\rm AH}} \frac{\mathrm{d}z}{\mathrm{d}r} = \lim_{r\to r_{\rm AH}} \frac{\big(3-2kr^2\big)\,(1+z)}{r\,(1-kr^2+\mathcal{G})}. \tag{12.5}$$

Using this, $\lim_{r\to r_{\rm AH}}(B_2/B_3)$ can be easily calculated from (11.12), and the result used in (11.14), to find

$$\lim_{r\to r_{\rm AH}} \frac{\mathrm{d}t_B}{\mathrm{d}r} = \lim_{r\to r_{\rm AH}} \frac{2\mathcal{D}\sqrt{1-kr^2}}{H_0 r(1+z)}\left(\frac{3-2kr^2}{1-kr^2+\mathcal{G}}-1\right). \tag{12.6}$$

Equation (9.8) is one more control value at the AH.

XIII. THE LIMITS OF (11.12) AND (11.14) AT $r \to 0$

Expressions of the form $0/0$ also appear at $r = 0$. From (8.2) one finds, using $\Omega_m + \Omega_\Lambda \equiv 1$

$$\lim_{r\to 0} \frac{\mathcal{D}}{r} = \lim_{r\to 0} \frac{\mathrm{d}z}{\mathrm{d}r} \stackrel{\text{def}}{=} X. \tag{13.1}$$

Anticipating that $X \neq 0$, so that $\lim_{r\to 0}\left(r^3/\mathcal{D}\right) = 0$, one finds from (9.2), (9.5), (11.10) and (11.13)

$$\lim_{r\to 0} A_1 = \lim_{r\to 0} A_2 = \lim_{r\to 0} B_2 = -1, \tag{13.2}$$

$$\lim_{r\to 0} \frac{r}{A_2+1} = \sqrt{\frac{X}{2M_0H_0}}, \tag{13.3}$$

$$\lim_{r\to 0} (rB_3) = -\frac{1}{2X} - \sqrt{\frac{X}{2M_0H_0}}\,\sqrt{1-\frac{kX}{2M_0H_0}}. \tag{13.4}$$

Taking the limit of (11.12) at $r \to 0$, then using (13.2) – (13.4), we obtain

$$X^3 + kX - 2M_0H_0 = 0. \tag{13.5}$$

This equation, irrespectively of the value of k, has only one solution such that $X > 0$; a proof is given in Appendix C.[7] This solution is located in (U_1, U_2), where

$$U_1 = (2M_0H_0)^{1/3}, \tag{13.6}$$

$$U_2 > \sqrt{-k/3} + \max\left\{(2M_0H_0)^{1/3}, \sqrt{-2k}/3\right\}.$$

[7] $\lim_{r\to 0} \mathrm{d}z/\mathrm{d}r < 0$ would mean that $z < 0$ in a vicinity of the observer, i.e., that the Universe locally collapses upon her. While this happens in certain inhomogeneous models, this cannot happen in a model designed to mimic RW.

Using (13.5) back in (13.4) we obtain

$$\lim_{r\to 0} (rB_3) = -\frac{3}{2X} + \frac{k}{2M_0H0}. \tag{13.7}$$

From (8.1) and (13.1) we have

$$\lim_{r\to 0} \frac{R_{\rm ng}}{r} = \lim_{r\to 0} \frac{\mathcal{D}}{H_0 r(1+z)} = \frac{X}{H_0}, \tag{13.8}$$

and then from (11.5) – (11.6)

$$\mathcal{T} \stackrel{\text{def}}{=} t(0) - t_B(0) = \frac{M_0}{(-k)^{3/2}}\left[\sqrt{\mathcal{Y}^2-1} - \ln\left(\mathcal{Y}+\sqrt{\mathcal{Y}^2-1}\right)\right], \tag{13.9}$$

where

$$\mathcal{Y} \stackrel{\text{def}}{=} 1 - \frac{kX}{M_0H_0}. \tag{13.10}$$

The $\mathcal{T}$ in (13.9) is the age of the Universe at $r = 0$.

From (11.14) we can further calculate

$$\lim_{r\to 0} \frac{\mathrm{d}t_B}{\mathrm{d}r} = \frac{M_0X}{2\,(3M_0H_0 - kX)} \times \left[3\,(\Omega_m - 1) - \frac{kX}{M_0H_0}\left(\frac{3}{2}\,\Omega_m - 1\right)\right]. \tag{13.11}$$

This calculation is tricky, so it is presented in Appendix D. With $k < 0$ and $\Omega_m = 0.32$, the limit (13.11) is negative, so $t_B(r)$ will be a decreasing function of r at least in some neighbourhood of $r = 0$.

XIV. THE AGE OF THE UNIVERSE AND THE VALUE OF k

The numerical values of the constants that will appear in the calculations are given by (10.1).

Before proceeding to solve (11.12), a value for k must be chosen. That value determines the age of the Universe at the center, via (13.9) and (13.10). It is to be noted that X, given by (13.5), is a function of k. For $k < 0$, $X > (2M_0H_0)^{1/3}$ must hold, and X monotonically increases from $(2M_0H_0)^{1/3}$ at $k = 0$ to $+\infty$ at $k \to -\infty$ (but $\mathrm{d}X/\mathrm{d}k \underset{k\to-\infty}{\longrightarrow} 0$).

For the function $\mathcal{T}(k)$ given by (13.9) we find

$$\lim_{k\to 0} \mathcal{T} = \frac{2}{3H_0}, \qquad \lim_{k\to-\infty} \mathcal{T} = \frac{1}{H_0} \tag{14.1}$$

$$\lim_{k\to-\infty} \frac{\mathrm{d}\mathcal{T}}{\mathrm{d}k} = 0. \tag{14.2}$$

The graph of $\mathcal{T}(-k)$ is shown in Fig. 10. As can be seen, $\mathcal{T}(-k) < 1/H_0$ everywhere. However, in the L–T model, the "age of the Universe" is different at every r. The point, at which the L–T age can be compared to that of ΛCDM is the intersection of the past light cone of the

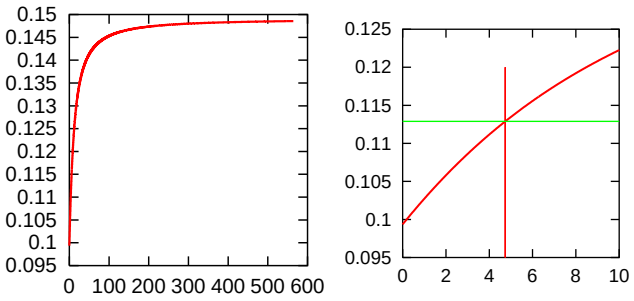

FIG. 10: **Left panel:** Graph of the function $\mathcal{T}(-k)$. It has the upper bound $1/H_0$. **Right panel:** A closeup view of the same graph over a smaller range of k. The vertical line marks the value $k = -4.7410812$ chosen in numerical experiments (see text), the horizontal line marks the associated age of the Universe at the center $\mathcal{T}(0) = 0.1128971437689653$ NTU.

L–T observer with the Big Bang. This is the place that the observer can (in principle) see and infer something about, not the central age given by (13.9) – (13.10). The L–T age at that point (call it "edge age") could be assumed equal to (10.9), and the corresponding value of k could then be determined in numerical experiments. This can be done by assuming a value for $\mathcal{T}$, calculating k from (13.9) – (13.10), then solving (11.12) – (11.15), and deducing a correction to the chosen value of $\mathcal{T}$.

But it turns out that a preferred unique value of k emerges already by integrating (11.12) (or (11.15)). With k off the preferred value, the function $z(r)$ found by integrating (11.15) backward from $r = r_{\rm AH}$, misses the point $(r, z) = (0, 0)$. The k fine-tuned to ensure that $z(0) = 0$ implies the edge age close to (10.9).

However, there is a problem here. Similarly to what has been said above, when k is off the opitmal value, $z(r)$ found by integrating (11.12) forward from $r = 0$, misses the point $(r, z) = (r, z)_{\rm AH}$. The k that ensures maximal precision at $r = 0$ is -4.74061, the one that ensures maximal precision at $r_{\rm AH}$ is -4.7410812. A preference was given to maximal precision at $r_{\rm AH}$. So, the k fine-tuned to $z_{\rm AH}$ and its associated X (found from (13.5) by the bisection method) are[8]

$$k = -4.7410812, \qquad X = 3.028567231968699. \quad (14.3)$$

XV. NUMERICAL CALCULATION OF $z(r)$ FROM (11.12)

The precision in calculating $z(r)$ and $t_B(r)$ depends on the precision in determination of the function $\mathcal{D}(z)$ and of the values of $\mathcal{D}$ and z at the AH. So, first, a Fortran 90 program was used to determine $\mathcal{D}(z)$ for any z by calculating the integral in (8.2) with the step $\mathrm{d}z' = z_{\rm max} \times 10^{-9}$ (the same program that produced the data for Fig. 9, but more precise) up to $z_{\rm max} = 1.585$ – slightly above the $z_{\rm AH}$ from Fig. 9. This program found the values of $z_{\rm AH}$ and $\mathcal{D}_{\rm AH}$ (at which $A_1 = 0$) to be

$$1.582432259768032 < z_{\rm AH} < 1.582432261353032,$$
$$1.037876550094136 < \mathcal{D}_{\rm AH} < 1.037876550731146. \quad (15.1)$$

These lower limits of $z_{\rm AH}$ and $\mathcal{D}_{\rm AH}$ were provisionally taken as their true values. The interval $Z \stackrel{\rm def}{=} [0, z_{\rm AH}]$ was divided into 10^5 segments, for each $z_i \in Z$, $i = 0, \ldots, 10^5 - 1$ the value of $\mathcal{D}(z_i)$ was found, and the $(z_i, \mathcal{D}_i)$ were tabulated. Numerical errors caused that the last value of z in the table was larger than the upper limit in (15.1). Consequently, the penultimate values of z and $\mathcal{D}$ were taken as defining the AH, they are

$$(z, \mathcal{D})_{\rm AH} = (1.582430687623614, 1.037876401742206), \quad (15.2)$$

and they are both lower than the lower limits in (15.1). The corresponding $r_{\rm AH}$ was calculated from (9.4):

$$r_{\rm AH} = 0.3105427968086945. \quad (15.3)$$

The table of values of $\mathcal{D}(z)$ was then used in integrating (11.15) numerically backward from $z = z_{\rm AH}$ to $z = 0$.

Since $z \to \infty$ at the Big Bang, z is not a usable parameter in the vicinity thereof, and $\mathcal{D}(z)$ cannot be tabulated in that region. The value of r, at which the Big Bang would be reached, was not known in advance, so it took some experimenting to determine the step $\Delta r = 2.4 r_{\rm AH} \times 10^{-5}$ and the number of steps $N = 15 \times 10^4$. For each $r > r_{\rm AH}$, the corresponding z was calculated by integrating (11.12) forward, with the initial condition (15.2), and the corresponding $\mathcal{D}(z)$ was found from

$$\mathcal{D}(z + \Delta z) = \mathcal{D}(z) + \frac{\Delta z}{\sqrt{\Omega_m (1 + z')^3 + \Omega_\Lambda}}, \quad (15.4)$$

which is a consequence of (8.2). The biggest values of (r, z) that the program could yet handle were

$$(r, z)_{\rm BB} = (1.422005301219788\,, \\ 1.6236973619875722 \times 10^{229})\,. \quad (15.5)$$

The $r_{\rm BB}$ was taken to be at the intersection of the observer's past light cone with the Big Bang.

The resulting function $z(r)$ is presented in Fig. 11; for later reference it will be denoted by $z_{\rm back}(r)$. The main graph shows $z(r)$ for $r \in [0.0, 0.5]$ (the lower curve). The upper curve is the function $z_\Lambda(r)$ of the ΛCDM model, calculated from (6.1), (4.4) and (2.16). The right curve in the inset is $z(r)$ for $r \in [0.3, 1.3]$, i.e. from the neighbourhood of the AH to a value at which z begins to grow very fast. The left curve is $z_\Lambda(r)$ in the same range of

[8] These numbers, and several other numbers displayed further on, may look to be excessively precise. They are indeed – for astrophysical applications. However, to avoid misalignments in some of the graphs, the numbers resulting from numerical programs are quoted as provided by Fortran90 at "double precision".

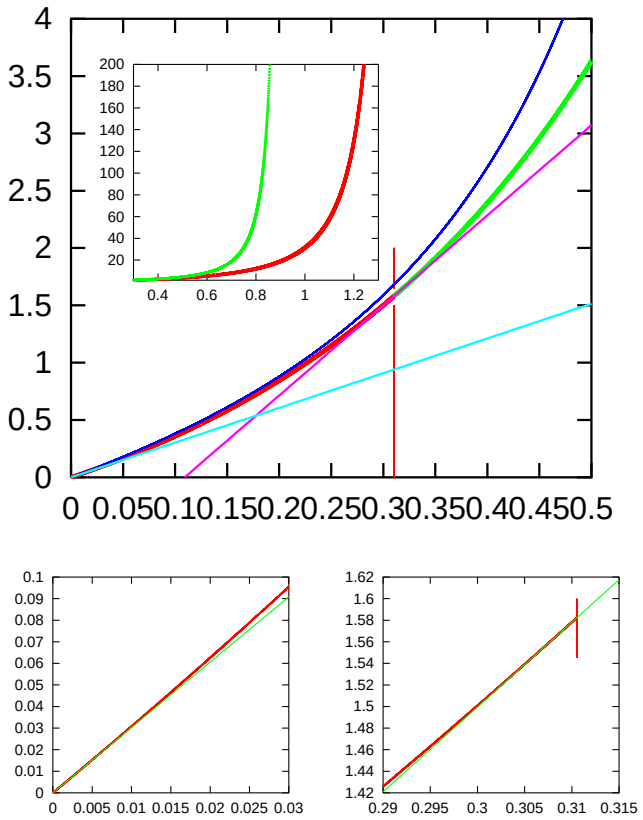

FIG. 11: The lower curve in the large panel is the graph of $z(r)$ calculated by integration of (11.15) backward and of (11.12) forward from the AH, with $k = -4.7410812$. The upper curve is the function $z_\Lambda(r)$ of the ΛCDM model. The vertical line marks $r = r_{\rm AH}$ given by (15.2). The sloping straight lines are tangents to $z(r)$ at $r = 0$ and at $r = r_{\rm AH}$ calculated from (13.5) and (12.5), respectively. The right curve in the inset is $z(r)$ for $r > r_{\rm AH}$. The left curve is the corresponding segment of $z_\Lambda(r)$. The two lower panels show closeup views of the neighbourhood of $r = 0$ (left) and of $r = r_{\rm AH}$ (right). The vertical stroke in the right panel marks $r = r_{\rm AH}$.

r. The panels below the main graph show that $z(r)$ respects the slopes given by (13.5) and (12.5) at $r = 0$ and $r = r_{\rm AH}$, respectively, with a satisfactory precision.

As seen from Fig. 11, the functions $z(r)$ in the L–T model and in the ΛCDM model are different. In particular, $z_\Lambda(r) \to \infty$ at $r = 0.9098426708844661 < r_{\rm BB}$. Thus, this time it should not be expected that the light cone of the L–T model will coincide with that of ΛCDM. The aim here is not to duplicate the light cone, but the $D_L(z)$ relation (2.20) via (2.14).

In order to verify the precision of the algorithm, the calculation of $z(r)$ was repeated by a different method. Namely, (11.12) was integrated from $r = 0$ up to a point close behind the AH. For each z, the associated value of $\mathcal{D}$ was calculated from (15.4). The number of steps was 11×10^4, and the size of the step was $\Delta r = 10^{-5} r_{\rm AH}$.

A problem occurred near $r = r_{\rm AH}$. Namely, because of numerical errors, A_2 became zero at a smaller r than A_1, even though each of them is supposed to become zero at $r = r_{\rm AH}$. As a result, in the range where $A_2 > 0$ (and thus $B_2 > 0$) while $A_1 < 0$, $\mathrm{d}z/\mathrm{d}r$ calculated by the program became negative and could not return to positive values when the calculation was continued. Thus, the program was designed to stop once A_2 becomes positive. The function thus obtained will be denoted $z_{\rm forw}(r)$.

At the scale of Fig. 11, the graphs of $z_{\rm forw}(r)$ and $z_{\rm back}(r)$ coincide. Near $r = 0$ they differ by $\Delta z \approx 7.35 \times 10^{-4}$; see the left panel of Fig. 12. As explained in Sec. XIV, the precision in that area could be improved to 0.5×10^{-7}, but this would cause a worse precision at the AH, where the difference between the two curves is $\Delta z \approx 0.5 \times 10^{-6}$. The right panel shows that area; at that scale the end points of the two curves seem to coincide.

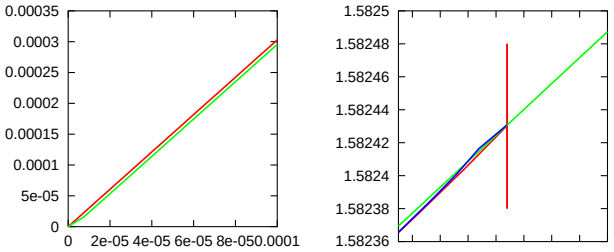

FIG. 12: Comparison of $z_{\rm back}(r)$ and $z_{\rm forw}(r)$. **Left panel:** closeup view of the segment $r \in [0, 10^{-4}]$. The upper line is $z_{\rm forw}(r)$; the lower line is $z_{\rm back}(r)$. **Right panel:** closeup view of the vicinity of $r = r_{\rm AH}$ ($r_{\rm AH}$ is marked with the vertical stroke). The sloping straight line is the tangent given by (12.5). The broken line is $z_{\rm back}(r)$. The third line is $z_{\rm forw}(r)$; at the scale of this figure it seems to hit the end point $(r_{\rm AH}, z_{\rm AH})$ exactly. The tics on the horizontal axis go from 0.310536 to 0.310550 and are separated by $\Delta r = 2 \times 10^{-6}$.

XVI. NUMERICAL CALCULATION OF $t_B(r)$ FROM (11.14)

Several quantities in (11.14) tend to zero as $r \to 0$. It is important not to let the numerical program divide a finite quantity by one that tends to zero. Consequently, it is advantageous to rearrange (11.14) by introducing new quantities as follows, using (11.13) and (11.9):

$$F_1 \stackrel{\rm def}{=} \mathcal{D}/r \underset{r\to 0}{\longrightarrow} X, \tag{16.1}$$

$$F_2 \stackrel{\rm def}{=} \frac{F_1}{2M_0H_0(1+z)}, \tag{16.2}$$

$$F_3 \stackrel{\rm def}{=} \sqrt{1 - kF_2}, \tag{16.3}$$

$$rB_3 \stackrel{\rm def}{=} F_4 = \frac{A_1}{2F_1} + B_2\sqrt{F_2}F_3, \tag{16.4}$$

$$F_5 \stackrel{\rm def}{=} \frac{\sqrt{F_2}}{H_0(1+z)F_3F_4}, \tag{16.5}$$

$$\mathcal{D}B_3 - A_1\left[\frac{3}{2} - \frac{kr^2}{(A_2+1)^2}\right] \stackrel{\text{def}}{=} F_6 \tag{16.6}$$

$$= F_3\left[-F_1\sqrt{F_2}\sqrt{1-kr^2} + F_3\frac{1+z}{\sqrt{\Omega_m(1+z)^3+\Omega_\Lambda}}\right],$$

$$\frac{\mathrm{d}t_B}{\mathrm{d}r} = F_3F_5\left(\frac{F_6}{r}\right). \tag{16.7}$$

Of the quantities defined above, F_1 and (F_6/r) behave as $0/0$ at $r=0$. However, $\lim_{r\to 0}F_1$ is given by (13.1) and (13.5), and the value of F_1 at the first grid point after $r=0$ is calculated without problems using (11.12). Given F_1, the values of $F_2,\ldots,F_5$ at $r=0$ are well-defined, and the only remaining $0/0$ expression is F_6/r.

The parametrisation (16.1) – (16.6) works well in a neighbourhood of $r=0$. At $r=r_{\rm AH}$ other quantities in (11.4) tend to zero (they are A_1, A_2, B_2 and B_3), and another rearrangement minimises numerical errors:

$$G_1 \stackrel{\text{def}}{=} A_2/A_1, \tag{16.8}$$

$$G_2 \stackrel{\text{def}}{=} \sqrt{(A_2+1)^2 - kr^2}, \tag{16.9}$$

$$G_3 \stackrel{\text{def}}{=} \sqrt{1-kr^2}, \tag{16.10}$$

$$G_4 \stackrel{\text{def}}{=} H_0(1+z)G_2, \tag{16.11}$$

$$\frac{B_3}{A_1} \stackrel{\text{def}}{=} G_5 = \frac{1}{2\mathcal{D}} + \frac{G_1G_2\,(A_2+2)}{(A_2+1)^2\,(G_2+G_3)}, \tag{16.12}$$

$$\frac{\mathrm{d}t_B}{\mathrm{d}r} = \frac{1}{rG_4}\left\{\mathcal{D} - \frac{1}{G_5}\left[\frac{3}{2} - \frac{kr^2}{(A_2+1)^2}\right]\right\}. \tag{16.13}$$

A similar rearrangement must be made in (11.12),

$$\frac{B_2}{A_1} \stackrel{\text{def}}{=} G_6 = \frac{A_2+2}{G_2+G_3}\,G_1, \tag{16.14}$$

$$\frac{rB_3}{B_2} \stackrel{\text{def}}{=} G_7 = \frac{r}{2\mathcal{D}G_6} + \frac{rG_2}{(A_2+1)^2}, \tag{16.15}$$

$$\frac{\mathrm{d}z}{\mathrm{d}r} = \frac{1+z}{G_3G_7}\left[\frac{3}{2} - \frac{kr^2}{(A_2+1)^2}\right]. \tag{16.16}$$

The only quantity in (16.8) – (16.16) that behaves like $0/0$ at $r\to r_{\rm AH}$ is G_1. The G_2, G_3 and G_4 have well-defined values at $r_{\rm AH}$, and once G_1 is calculated, G_5, G_6 and G_7 have values at $r_{\rm AH}$, too. Experiment showed that the program handles G_1 without any fluctuations.

It would be natural to combine the two rearrangements so that as many occurrences of r as possible in (16.8) – (16.16) cancel out, thus hopefully improving the accuracy of this parametrisation near $r=0$. Such an experiment was done, but it did not lead to the intended improvement – the graph of $t_B(r)$ did not change.

The limit of $(\mathrm{d}t_B/\mathrm{d}r)$ at $r\to r_{\rm AH}$ is given by (12.6), but $t_B(r_{\rm AH})$ cannot be calculated independently of (11.14). The integration of (16.7) must thus begin at $r=0$, and $t_B(r_{\rm AH})$ is found in the process. The $t_B(0)$ is given by (13.9), with $t(0)=0$ by assumption.

Equation (16.7) was integrated from $r=0$ to $r=r_{\rm AH}$ by using the tabulated values of z and $\mathcal{D}$, with $r(z)$ calculated along the way from (11.15). A continuation of $t_B(r)$ for $r>r_{\rm AH}$ was found by integrating (16.13) and calculating the values of z and $\mathcal{D}$ from (11.12) and (15.4), respectively. The initial point for the continuation was corrected as described further on. Figure 13 shows the resulting $t_B(r)$, together with the tangents at $r=0$ and $r=r_{\rm AH}$, and with the vertical line marking $r=r_{\rm AH}$.

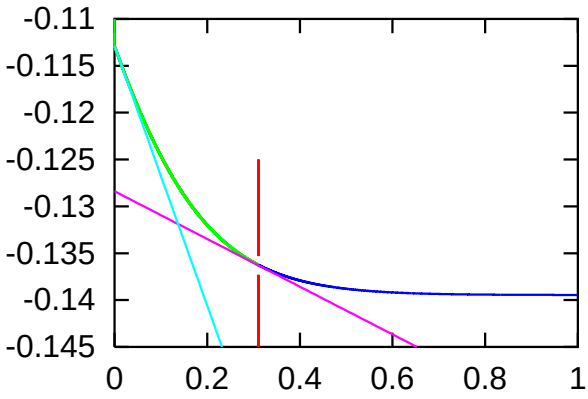

FIG. 13: The function $t_B(r)$ calculated by integrating (16.7) from $r=0$ to $r=r_{\rm AH}$ and by integrating (16.13) beyond $r=r_{\rm AH}$. The stroke marks $r=r_{\rm AH}$. The sloping straight lines are the tangents to $t_B(r)$ at $r=0$ and at $r=r_{\rm AH}$ calculated from (13.11) and (12.6), respectively. The curve found by integrating (16.13) backward from $r=r_{\rm AH}$ is also present in the figure, but, at this scale, it coincides with the $r<r_{\rm AH}$ part of first curve. The discrepancies between the two curves are shown in Figs. 14 and 15.

In order to verify the calculation of $t_B(r)$, (16.13) was integrated backward from $r=r_{\rm AH}$, with the initial value $t_B(r_{\rm AH})$ corrected as described below. The resulting curve is also shown in Fig. 13, but, at this scale, looks to coincide with the former one. Figures 14 and 15 display the discrepancies between the two integrations. As seen in the main graph of Fig. 14, the integration backward from $r_{\rm AH}$ gives a large discrepancy with the initial data at $r=0$ given by (13.9) and (13.11). At $r\approx 0.002$ the difference is $\Delta t_B \approx 2.0\times10^{-5}$ NTU $\approx 1.96\times10^6$ years. The inset in Fig. 14 displays an even closer look at the neighbourhood of $r=0$. It shows the forward-integrated $t_B(r)$ (the lower curve) and its tangent calculated from (13.11). Numerical instabilities cause that the curve departs from the right slope already at the first grid point, but the resulting difference $\Delta t_B < 0.3\times10^{-7}$ NTU ≈ 2940 years, which is cosmologically insignificant.

Figure 15 shows the neighbourhood of $r=r_{\rm AH}$ in Fig. 13. The $t_B(r)$ found by integrating (16.7) forward from $r=0$ is the lower curve left of the vertical stroke, which marks $r=r_{\rm AH}$. It misses the correct slope at $r_{\rm AH}$ – the tangent at $r_{\rm AH}$, calculated from (12.6), is the sloping straight line. (This means it also missed the correct value

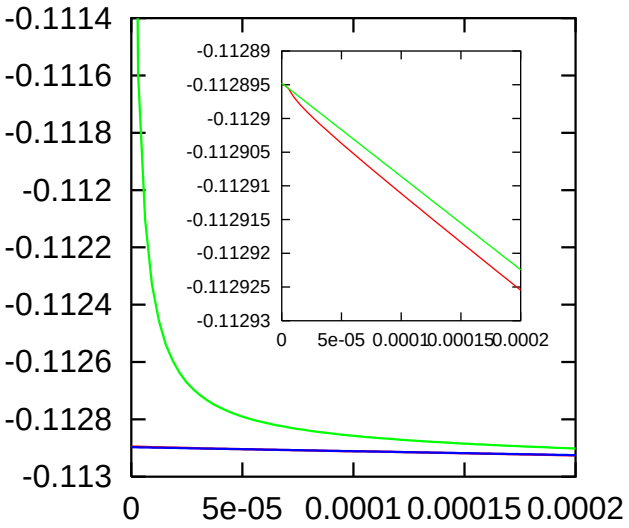

FIG. 14: Closeup view of the neighbourhood of $r = 0$ in Fig. 13. The upper curve in the main graph is $t_B(r)$ calculated by integrating (16.13) backward from $r = r_{\rm AH}$. The lower curve is obtained by integrating (16.7) forward from $r = 0$; at this scale, within the figure, it coincides with its tangent given by (13.11). The inset shows that the lower curve departs from the correct slope already at the first grid point, but this leads to the difference $\Delta t_B < 0.3 \times 10^{-7}$ NTU ≈ 2940 years.

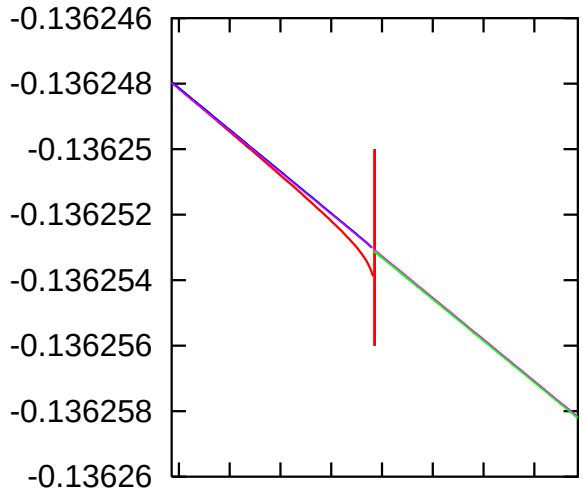

FIG. 15: Closeup view of the curves from Fig. 13 in the neighbourhood of $r = r_{\rm AH}$ (marked by the vertical stroke). The sloping straight line is the tangent from (12.6). The $t_B(r)$ curves, calculated by integrating (16.13) forward and backward from $r = r_{\rm AH}$, coincide at this scale with the tangent. Their initial point had to be set by hand as described in the text. The lower curve left of $r_{\rm AH}$ is the $t_B(r)$ found by integrating (16.7) forward from $r = 0$. It misses the slope at $r = r_{\rm AH}$ given by (12.6). The tics on the horizontal axis go from 0.31035 to 0.3107 with the interval $\Delta r = 5 \times 10^{-5}$.

at $r_{\rm AH}$, but this cannot be calculated independently.) However, it coincides with that tangent in a certain range of r, so the intersection of the tangent with $r = r_{\rm AH}$ at $t = -0.1362530696173036$ was assumed to be the correct end point $t_B(r_{\rm AH})$. This end point was then used as the initial point for the integration of (16.13) forward and backward from $r = r_{\rm AH}$. Both integrations avoided numerical instabilities. At the scale of Fig. 15, these curves coincide with the tangent.

The graphs indicate that $t_B(r)$ is a decreasing function in the whole range, so no shell crossings are present.

XVII. NUMERICAL CALCULATION OF THE LIGHT CONE

With $t_B(r)$ now given, eq. (11.2) can be numerically solved. Substituting (11.4) in (11.2), using (8.1) – (8.2) for R, and then using (16.1) – (16.3) we obtain

$$\frac{{\rm d}t}{{\rm d}r} = \frac{1}{\sqrt{1-kr^2}} \left[-\frac{F_1}{H_0(1+z)} + r\frac{{\rm d}t_B}{{\rm d}r}\frac{F_3}{\sqrt{F_2}} \right]. \qquad (17.1)$$

This is well-behaved at $r = 0$ and at $r = r_{\rm AH}$. The values of $t_{B,r}(r)$ were found in integrating (16.7) and (16.13).

The resulting light cone profile is shown in Fig. 16, compared with the light cone of the ΛCDM model. The two light cones, as predicted, do not coincide. In particular, the L–T light cone is everywhere later than the ΛCDM cone, and the difference in time increases as the Big Bang is approached. The L–T light cone meets the Big Bang at a larger value of r, which was seen already in Fig. 11. It touches the $t_B(r)$ curve horizontally, as it should (see Sec. VII). However, $t_B(r)$ asymptotes to a later value of t than the ΛCDM Big Bang, namely to $t = -0.139$ NTU. In consequence, up to a certain $r > r_{\rm AH}$, the L–T Universe is everywhere younger than ΛCDM. The difference in the bang times at the edge of the figure is $\Delta t \approx 0.002$ NTU $\approx 1.96 \times 10^8$ y.

One might suspect that the disagreement between the two light cones is a consequence of numerical errors. In truth, the numerical error is much smaller, as shown by the final test: the two sides of eq. (8.1) were compared numerically. The right-hand side, the function $F_r(r) \stackrel{\rm def}{=} \mathcal{D}/[H_0(1+z)]$, is calculated directly from the input data. The left-hand side, the function $F_l(r) \stackrel{\rm def}{=} R(t_{\rm ng}(r), r)$, depends on the whole chain of numerical calculations that were carried out to find $t(r)$. The $F_r(r)$ was calculated on top of $z_{\rm back}(r)$, see Sec. XV. The $F_l(r)$ was calculated on top of $t(r)$ and $t_B(r)$. Each time when t and t_B were found for a given r, the corresponding $\eta(r)$ in (2.7) was found by the bisection method (with the precision $\Delta\eta = 10^{-15}$), and then the $R(t(r), r)$ was calculated from the first of (2.7).

Figure 17 shows the comparison. The upper panel shows the two functions in full range; at this scale they seem to coincide, except that $R_l(r)$ ends at a smaller r. The lower left panel shows numerical errors at the maximum. There is a discontinuity in $F_l(r) = R(t(r), r)$

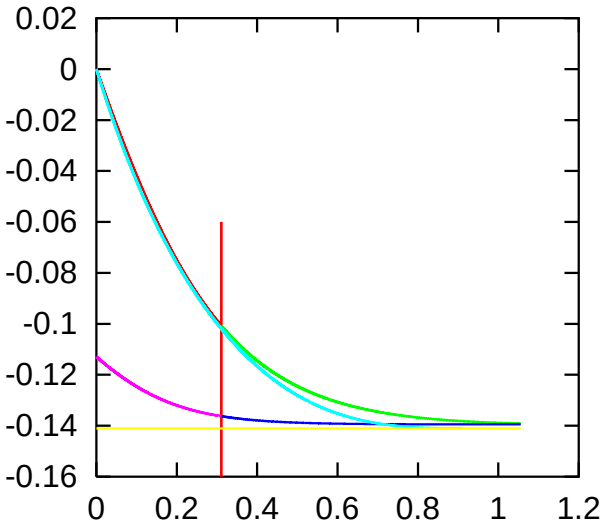

FIG. 16: The past light cone of the central observer in the L–T model that duplicates the relation (8.1) (the uppermost curve) compared with that of the ΛCDM model (4.4) (the lower curve, partly nearly coincident with the first one). The lowest curve is the $t_B(r)$ from Fig. 13, the horizontal straight line marks the Big Bang of the ΛCDM model, given by (10.10). The vertical line marks $r = r_{\rm AH}$.

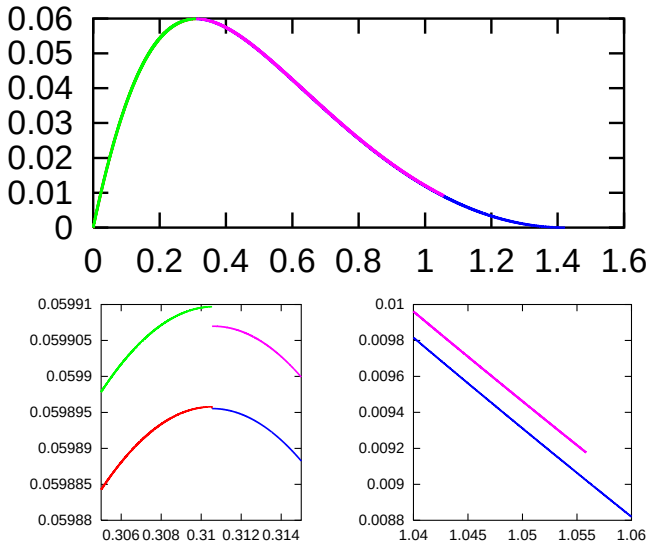

FIG. 17: **Upper panel:** Comparison of the two sides of eq. (8.1). At this scale, the two functions seem to coincide. **Lower left panel:** closeup view of the maximum in the upper panel. The upper curve is $F_l(r)$, the lower curve is $F_r(r)$. The graph shows the discontinuities at the maximum that resulted from numerical errors. **Lower right panel:** the functions $F_l(r)$ (upper line) and $F_r(r)$ (lower line) at the right end of F_l. See text for more explanation.

equal to $\approx 2.78 \times 10^{-6}$ NLU ≈ 83.5 kpc $\approx 2.72 \times 10^5$ y, a discontinuity in $F_r(r)$, equal to 10^{-7} NLU ≈ 3 kpc ≈ 9800 y, and the difference between $R_l(r)$ and $R_r(r)$, which, at the maximum, is $\approx 1.39 \times 10^{-5}$ NLU ≈ 417 kpc $\approx 1.36 \times 10^6$ y. The lower right panel shows the same difference at the right end of the graph of $R_l(r)$, which is $\approx 1.44 \times 10^{-4}$ NLU ≈ 4.32 Mpc $\approx 1.41 \times 10^7$ y.

In summary: we required that the L–T model with $\Lambda = 0$, $2E/r^2 = -k =$ constant and variable $t_B(r)$ duplicates the $D_L(z)$ function given by (2.20) via (2.14). Under these assumptions, the values of $H_0 = 67.1$ km/(s $\times$ Mpc) and the age of the Universe $T = 13.819 \times 10^9$ y taken from observations [3] determine the value of k, and then the shape of $t_B(r)$ is determined such that it mimics the effect of Λ on a single light cone.

Thus, using the $\Lambda = 0$ L–T model with constant $E/r^2 > 0$, one can explain away the accelerated expansion of the Universe as follows. In the ΛCDM model, the bang time is constant, while in the L–T model the Big Bang occurs progressively later when the position of the observer is approached. Consequently, the time between the Big Bang and the instant of crossing the observer's past light cone becomes progressively shorter in L–T than in ΛCDM. Because of this, the expansion velocity of matter in the L–T model, at the points of intersection with this cone, is everywhere greater than in a Friedmann model with $\Lambda = 0 = k$, and the difference is increasing toward the observer, similarly to what happens in Fig. 5. Thus, accelerating expansion is mimicked: instead of increasing with time, the excess expansion velocity increases with position in space.

This may look artificial (the observer being placed at that r, where $t_B(r)$ is greatest). But it should be noted that the model that led to this conclusion had from the beginning a built-in artificial assumption, made in order to simplify the calculations: the function E being the same as in the Friedmann model. This left the whole task of imitating acceleration to t_B alone. See also the comments in the next section.

XVIII. COMMENTS ON APPLICATIONS OF THE L–T MODEL TO COSMOLOGY

As has already been said, the L–T geometry cannot be taken as a model of the observed Universe at pre-recombination times: its built-in assumption $p = 0$ becomes strongly unrealistic there. Unfortunately, several papers were published, in which the authors tried to discredit the L–T model by doing just that. One of the persistent legends says that a realistic L–T model must have constant t_B. This crippling limitation allegedly must be made because $\mathrm{d}t_B/\mathrm{d}r \neq 0$ generates decreasing density perturbations, and they would imply "extreme" inhomogeneity at early times [29]. This, the argument goes, would contradict the predictions of inflation.

Formally, the decreasing density perturbation becomes infinite as $t \to t_B$ [11]. However, this would be a problem for cosmology if the L–T model would be supposed to apply all the way to $t = t_B$, which is not the case. The direct connection between the decreasing density perturbation and $\mathrm{d}t_B/\mathrm{d}r \neq 0$ was demonstrated only for the L–T and Szekeres [30] models (by Silk [31] and

Goode and Wainwright [32], respectively, see Ref. [11] for short descriptions). In a more general model, still unknown, which should apply before recombination, the corresponding connection may be indirect, and need not imply infinite perturbations close to the Big Bang. And, let us remember, the Big Bang itself is an artifact of general relativity that is supposed to go away when quantum gravity provides the right description of that epoch.

Another legend says that an L–T model mimicking accelerated expansion must contain a void around its center of symmetry. Our result (13.11), from which it follows that $\lim_{r\to 0} \mathrm{d}t_B/\mathrm{d}r < 0$, provides a counterexample to this claim. Namely, from (2.8), knowing that $\lim_{r\to 0} M = \lim_{r\to 0} R = 0$, we find

$$\lim_{r\to 0} \frac{R^3}{M} = \lim_{r\to 0} \frac{3R^2 R_{,r}}{M_{,r}} = \frac{6}{\kappa\rho(t,0)} \stackrel{\mathrm{def}}{=} \frac{6}{\kappa\overline{\rho}}. \qquad (18.1)$$

Then, using (2.9), (11.4) and (18.1) in (2.8), we obtain

$$\lim_{r\to 0} (\kappa\rho_{,r}) = \frac{4(\kappa\overline{\rho})^{4/3}}{(6M_0)^{1/3}} \sqrt{2M_0 \left(\frac{\kappa\overline{\rho}}{6M_0}\right)^{1/3} - k}\, \frac{\mathrm{d}t_B}{\mathrm{d}r} < 0. \qquad (18.2)$$

Hence, in this case there is a peak of density at $r = 0$.

Much effort has been spent in the literature on the attempts to "disprove" the L–T model by exploiting its spherical symmetry [33]. Consequently, it has to be reminded that this model is mainly used as an exercise to gain insight into a nontrivial geometry. This insight is then exploited in applying, for example, the Szekeres model [11, 30] to cosmological problems; see examples of such applications in Refs. [34] – [41]. The Szekeres model is a generalisation of L–T; it has no symmetry and is more complicated computationally. Therefore, insights gained from carrying out the L–T exercises are helpful.

More generally, the L–T and Szekeres models are not supposed to be *the* ultimate models of the whole Universe. They are to be understood as *exact perturbations* superimposed on the background Friedmann model, and can be sensibly applied only to the description of local structures, such as galaxy clusters or voids, see Refs. [42], [43] and [11, 14]. Consequently, in situations, in which perturbed Friedmann models are deemed adequate, the L–T and Szekeres models, when they are correctly understood and applied, can only be still more adequate, being exact solutions of Einstein's equations. If they are to become objects of the now-so-called "precision cosmology", then results of observations should give information on the shapes of their arbitrary functions. Outright rejection is not a constructive approach.

We will never know how good or how bad any given model is until we test it at full generality in as many situations as will be invented by anyone. This will help in constructing the next generation of still more precise models. Excluding elements of a model on the basis of a speculative competing hypothesis is not what serious science used to be about. And it is unethical to use arguments of this kind to reject papers submitted for publication, as sometimes happens.

The artificial elements of the model considered here (the $D_L(z)$ being reproduced only on a single past light cone, the cone reaching the Big Bang where $\mathrm{d}t_B/\mathrm{d}r = 0$) are present because it was designed to mimic the observations via their projection on the ΛCDM past light cone. They do not appear when the L–T model is directly adapted to observations. The point made in this paper is: using the L–T model, observations can be accounted for without introducing the dark energy.

The way, in which the $D_L(z)$ function was reproduced here is not the only one possible. Iguchi et al. [6] demonstrated that such a reproduction is also possible with constant t_B, and $E(r)$ designed to mimic the effect of Λ. This dual approach will be a subject of a similar analysis as done here in a future paper. It should be recalled once more that with both $E(r)$ and $t_B(r)$ being arbitrary, two sets of observational data can be reproduced [7].

Appendix A: Proof that (3.2) has a solution for every Λ

Consider the equation equivalent to (3.2)

$$F(R) \stackrel{\mathrm{def}}{=} \tfrac{1}{3}\Lambda R^3 + R - 2M = 0. \qquad (A1)$$

For $\Lambda = 0$ the solution $R = 2M$ obviously exists. In all models with $\Lambda > 0$ R is oscillating between $R = 0$ and a finite maximal value $R = R_m$.[9] At $R = R_m$, where $R_{,t} = 0$ in (2.2), the following holds

$$G(R_m) \stackrel{\mathrm{def}}{=} \tfrac{1}{3}\Lambda {R_m}^3 - 2ER_m - 2M = 0, \qquad (A2)$$

and there is only one value of $R_m > 0$ that obeys (A2). Thus, at $R = R_m$

$$F(R_m) = (2E + 1)R_m. \qquad (A3)$$

Since $2E + 1 \geq 0$ (see (2.3)), we have $F(R_m) \geq 0$, while at $R = 0$, $F(R) = -2M \leq 0$ ($F = 0$ only at the center, where $M = 0$). So, $F(R) = 0$ has a solution for every $\Lambda > 0$; the solution is $R = R_m$ where $E = -1/2$ and $R < R_m$ where $E > -1/2$. Consequently, an AH exists.

Now consider $\Lambda < 0$. For $0 > \Lambda > \Lambda_{\mathcal{E}} \stackrel{\mathrm{def}}{=} -8E^3/(9M^2)$ (the Einstein value, see Ref. [11]) the reasoning above still applies to the oscillating models. For non-oscillating models in the same range of Λ, the subcases $E < 0$ and $E \geq 0$ have to be considered separately. When $E < 0$, the value of R is always greater than the R_m given by (A2), so it follows that $F(R) = 0$ has no solutions in that range of R (but it had a solution in the range of oscillating models, so the statement being proven is not

[9] Recall: (2.2) has the same algebraic form for the L–T and Friedmann models. The proof that all models with $\Lambda > 0$ are oscillating had been given by Friedmann [44], see Ref. [11] (Friedmann's cosmological constant λ is related to our Λ by $\lambda = -\Lambda$).

contradicted). When $E \geq 0$, R changes between 0 and ∞, and the reasoning given below applies.

For $\Lambda = \Lambda_{\mathcal{E}}$ the situation is similar, except that there exists in addition the static Einstein model, but this does not contradict the statement being proven.

For $\Lambda < \Lambda_{\mathcal{E}}$, R necessarily varies between 0 and ∞. Then, from (A1), $F(0) = -2M \leq 0$, and

$$\mathrm{d}F/\mathrm{d}R = \Lambda R^2 + 1. \tag{A4}$$

This is zero at $R = \pm 1/\sqrt{-\Lambda}$, so F has a maximum at $R = 1/\sqrt{-\Lambda}$, and $F(1/\sqrt{-\Lambda}) = 4\sqrt{-\Lambda} - 2M$. This is positive in some range $M \in [0, \sqrt{-\Lambda})$, so $F(R) = 0$ has a solution in this range, i.e. an AH exists. □

Appendix B: Proof that the AH coincides with the set $R_{,tr} = 0$ only in exceptional cases

Calculating $R_{,tr}$ from (11.3) and taking the result at $R = 2M$, one obtains, using (2.2) with $\Lambda = 0$

$$R_{,tr}\,|_{\mathrm{AH}} = \left\{ \frac{E_{,r}}{2E}\sqrt{2E+1} \right. \tag{B1}$$
$$\left. + \frac{1}{4M}\left[\left(\frac{3}{2}\frac{E_{,r}}{E} - \frac{M_{,r}}{M}\right)(t - t_B) - t_{B,r}\right]\right\}_{\mathrm{AH}}.$$

For $E = 0$, the analogue of (11.3) is ([11], eq. (18.112))

$$R_{,r} = \frac{M_{,r}}{3M}\, R - \sqrt{\frac{2M}{R}}\, t_{B,r}. \tag{B2}$$

The cases $E > 0$, $E = 0$ and $E > 0$ must be considered separately. Only the case $E < 0$ is presented here; the corresponding result for $E > 0$ follows analogously, and the one for $E = 0$ follows easily from (B2).

For $E < 0$ one finds $(t - t_B)$ as a function of R from (2.5) and takes it at $R = 2M$, obtaining

$$(t - t_B)_{\mathrm{AH}} = \frac{M}{(-2E)^{3/2}}$$
$$\times \left[\arccos(1 + 4E) - 2\sqrt{-2E(1+2E)}\right] \tag{B3}$$

(the arccos is to be calculated for $0 \leq 1 + 2ER/M \leq \pi$, i.e. for the expanding phase of the Universe). After substituting this in (B1) the following is obtained

$$R_{,tr}\,|_{\mathrm{AH}} = \frac{t_{B,r}}{4M}$$
$$-\frac{1}{4(-2E)^{3/2}}\left(\frac{3}{2}\frac{E_{,r}}{E} - \frac{M_{,r}}{M}\right)\arccos(1 + 4E)$$
$$-\frac{1}{4E}\left(\frac{E_{,r}}{2E} - \frac{M_{,r}}{M}\right)\sqrt{2E+1}. \tag{B4}$$

The AH is a curve in the (t, r) plane, so if $R_{,tr} = 0$ should hold along the whole AH, (B4) would force a relation between M, E and t_B, thus reducing the number of arbitrary functions to 2. This means that $R_{,tr} = 0$ can hold along the AH only in special cases.

The corresponding equation for $E = 0$ is

$$t_{B,r} = 2M_{,r}/3, \tag{B5}$$

from (B2), and it also limits the generality of the model.

Note that (B4) and (B5) do not hold in the Friedmann model, where $M/r^3 = M_0$, $2E/r^2 = -k$ and t_B are constant. Thus, $R_{,tr}\,|_{\mathrm{AH}} \neq 0$ even in the Friedmann limit.

Appendix C: Proof that (13.5) has only one real solution $X > 0$

Let us write (13.3) as

$$f(X) \stackrel{\mathrm{def}}{=} X^3 + kX - b = 0, \tag{C1}$$

where $k < 0$ and $b \stackrel{\mathrm{def}}{=} 2M_0H_0 > 0$. The function $f(X)$ has a local maximum at $X_- = -\sqrt{-k/3} < 0$ and a local minimum at $X_+ = \sqrt{-k/3} > 0$. We have

$$f(X_+) = -\frac{2(-k)^{3/2}}{3\sqrt{3}} - b < 0, \tag{C2}$$

so there must be a zero of $f(X)$ in $(X_+, +\infty)$, and

$$f(X_-) = \frac{2(-k)^{3/2}}{3\sqrt{3}} - b. \tag{C3}$$

When $(f(X_-) < 0$, there are no more real zeros of $f(X)$. When $(f(X_-) = 0$, $X = X_-$ is a double real zero of $f(X)$, additional to that guaranteed by (C2). When $(f(X_-) > 0$, there are two more real zeros of $f(X)$. However, the additional zeros are at $X < 0$, since $f(0) < 0$. □

Appendix D: The derivation of (13.11)

Using (13.1) and (13.5) we find

$$\lim_{r\to 0}\sqrt{\frac{2M_0H_0r(1+z)}{\mathcal{D}} - k} = X. \tag{D1}$$

Using (13.7), (11.10), (9.5) and (D1) in (11.14) we obtain

$$\lim_{r\to 0}\frac{\mathrm{d}t_B}{\mathrm{d}r} = \frac{2M_0}{-3M_0H_0 + kX}\lim_{r\to 0}\left\{\frac{1}{r}\left[\mathcal{D}B_3 - \frac{3}{2}\,A_1\right.\right.$$
$$\left.\left. + \frac{kr^2A_1}{(A_2+1)^2}\right]\right\} \stackrel{\mathrm{def}}{=} \frac{2M_0}{-3M_0H_0 + kX}\,\mathcal{Z}. \tag{D2}$$

In what follows, two more new symbols will be used:

$$Q \stackrel{\mathrm{def}}{=} \frac{1}{\sqrt{\Omega_m(1+z)^3 + \Omega_\Lambda}}, \tag{D3}$$

$$\mathcal{U} \stackrel{\mathrm{def}}{=} \sqrt{\frac{2M_0H_0r(1+z)}{\mathcal{D}} - k}. \tag{D4}$$

After writing out B_3, A_1 and A_2 we find from (D2)

$$\mathcal{Z} = \lim_{r\to 0}\left\{\frac{1}{r}\left[(1+z)Q - \frac{k\mathcal{D}Q}{2M_0H_0r} - \frac{\mathcal{D}^2\sqrt{1-kr^2}\mathcal{U}}{2M_0H_0r^2(1+z)}\right]\right\}. \tag{D5}$$

The limit at $r\to 0$ of the expression in square brackets is zero, so we can apply the de l'Hôpital rule and obtain

$$\begin{aligned}\mathcal{Z} &= \lim_{r\to 0}\left\{\frac{\mathrm{d}z}{\mathrm{d}r}\left[Q - \frac{3}{2}\Omega_m(1+z)^3Q^3 + \frac{\mathcal{D}^2\sqrt{1-kr^2}\mathcal{U}}{2M_0H_0r^2(1+z)^2} - \frac{\mathcal{D}\sqrt{1-kr^2}}{2r(1+z)\mathcal{U}} + \frac{3}{4}\,k\Omega_m\frac{(1+z)^2\mathcal{D}Q^3}{M_0H_0r}\right]\right.\\ &\quad\left. + \frac{k\mathcal{D}^2\mathcal{U}}{2M_0H_0r(1+z)\sqrt{1-kr^2}}\right\}\\ &\quad + \lim_{r\to 0}\left[\frac{kQ}{2M_0H_0} - \frac{k\mathcal{D}\sqrt{1-kr^2}}{M_0H_0r(1+z)\mathcal{U}} + \frac{3\sqrt{1-kr^2}}{2\mathcal{U}}\right]\times\lim_{r\to 0}\left[\frac{1}{r}\,\left(\frac{\mathcal{D}}{r} - Q\frac{\mathrm{d}z}{\mathrm{d}r}\right)\right],\end{aligned} \tag{D6}$$

where the expression in the first two lines and the first limit in the third line can be readily calculated:

$$\mathcal{Z} = F_1 + \left(\frac{3}{2X} - \frac{k}{2M_0H_0}\right)\lim_{r\to 0}\left[\frac{1}{r}\,\left(\frac{\mathcal{D}}{r} - Q\frac{\mathrm{d}z}{\mathrm{d}r}\right)\right], \tag{D7}$$

where

$$F_1 \stackrel{\text{def}}{=} X\left[\frac{3}{2}\,(1-\Omega_m) - \frac{kX}{2M_0H_0}\left(1 - \frac{3}{2}\Omega_m\right)\right]. \tag{D8}$$

In (D7) we now substitute for $\mathrm{d}z/\mathrm{d}r$ from (11.12), then factor out $1/(rB_3)$ and use (13.7). The result is

$$\mathcal{Z} = F_1 - \lim_{r\to 0}\left\{\frac{\mathcal{D}B_3}{r} - \frac{QB_2(1+z)}{r\sqrt{1-kr^2}}\left[\frac{3}{2} - \frac{kr^2}{(A_2+1)^2}\right]\right\}. \tag{D9}$$

Comparing (D9) with (D2) we see that

$$\begin{aligned}&\mathcal{Z} = F_1 - \mathcal{Z}\\ &-\lim_{r\to 0}\left\{\frac{1}{r}\left[\frac{3}{2} - \frac{kr^2}{(A_2+1)^2}\right]\left[A_1 - \frac{QB_2(1+z)}{\sqrt{1-kr^2}}\right]\right\}.\end{aligned} \tag{D10}$$

The second factor in square brackets has the limit zero, the first one is finite. Consequently

$$\mathcal{Z} = \frac{1}{2}\,F_1 = \frac{1}{4}\,X\left[3\,(1-\Omega_m) - \frac{kX}{M_0H_0}\left(1 - \frac{3}{2}\Omega_m\right)\right]. \tag{D11}$$

Using this in (D2) we obtain (13.11). □

Acknowledgement. I thank Krzysztof Bolejko for several useful comments.

[1] S. Perlmutter, G. Aldering, G. Goldhaber, R. A. Knop, P. Nugent, P. G. Castro, S. Deustua, S. Fabbro, A. Goobar, D. E. Groom, I. M. Hook, A. G. Kim, M. Y. Kim, L. C. Lee, N. J. Nunes, R. Pain, C. R. Pennypacker, R. Quimby, C. Lidman, R. S. Ellis, M. Irwin, R. G. McMahon, P. Ruiz-Lapuente, N. Walton, B. Schaefer, B. J. Boyle, A. V. Filippenko, T. Matheson, A. S. Fruchter, N. Panagia, H. J. M. Newberg, and W. J. Couch, *Astrophys. J.* **517**, 565 (1999).

[2] A. G. Riess, A. V. Filippenko, P. Challis, A. Clocchiatti, A. Diercks, P. M. Garnavich, R. L. Gilliland, C. J. Hogan, S. Jha, R. P. Krishner, B. Leibundgut, M. M. Phillips, D. Reiss, B. P. Schmidt, R. A. Schommer, R. C. Smith, J. Spyromilio, C. Stubbs, N. B. Suntzeff, and J. Tonry, *Astron. J.* **116**, 1009 (1998).

[3] Planck collaboration, *Planck* 2013 results. XVI. Cosmological parameters. arXiv 1303.5076.

[4] G. Lemaître, *Ann. Soc. Sci. Bruxelles* **A53**, 51 (1933a); English translation, with historical comments: *Gen. Relativ. Gravit.* **29**, 637 (1997).

[5] R. C. Tolman, *Proc. Nat. Acad. Sci. USA* **20**, 169 (1934); reprinted, with historical comments: *Gen. Relativ. Gravit.* **29**, 931 (1997).

[6] H. Iguchi, T. Nakamura and K. Nakao, *Progr. Theor. Phys.* **108**, 809 (2002).

[7] M.-N. Célérier, K. Bolejko and A. Krasiński, *Astronomy and Astrophysics* **518**, A21 (2010).

[8] C. Quercellini, L. Amendola, A. Balbi, P. Cabella, M. Quartin, *Phys. Reports.* **521**, 95 – 134 (2012).

[9] R. A. Vanderveld, E. E. Flanagan, and I. Wasserman, *Phys. Rev.* **D74**, 023506 (2006).

[10] A. Krasiński, *Inhomogeneous Cosmological Models*, Cambridge University Press 1997, 317 pp, ISBN 0 521 48180 5.

[11] J. Plebański and A. Krasiński, *An Introduction to General Relativity and Cosmology.* Cambridge University

Press 2006, 534 pp, ISBN 0-521-85623-X.
[12] C. Hellaby and K. Lake, *Astrophys. J.* **290**, 381 (1985) + erratum *Astrophys. J.* **300**, 461 (1985).
[13] H. Bondi, *Mon. Not. Roy. Astr. Soc.* **107**, 410 (1947); reprinted, with historical comments, in *Gen. Relativ. Gravit.* **31**, 1777 (1999).
[14] K. Bolejko, A. Krasiński, C. Hellaby and M.-N. Célérier, Structures in the Universe by exact methods – formation, evolution, interactions. Cambridge University Press 2010, 242 pp, ISBN 978-0-521-76914-3.
[15] S. W. Hawking and G. F. R. Ellis, *The Large-scale Structure of Spaceetime*. Cambridge University Press 1973.
[16] A. Krasiński and C. Hellaby, *Phys. Rev.* **D69**, 043502 (2004).
[17] G. F. R. Ellis, in *Proceedings of the International School of Physics 'Enrico Fermi', Course 47: General Relativity and Cosmology*, ed. R. K. Sachs. Academic Press, New York and London (1971), pp. 104 – 182; reprinted as a Golden Oldie in *Gen. Relativ. Gravit.* **41**, 581 (2009).
[18] W. Rindler, *Mon. Not. Roy. Astr. Soc.* **116**, 662 (1956); reprinted as a Golden Oldie in *Gen. Relativ. Gravit.* **34**, 131 (2002).
[19] A. Krasiński, C. Hellaby, K. Bolejko and. M.-N. Célérier, *Gen. Relativ. Gravit.* **42**, 2453 (2010).
[20] A. Krasiński and K. Bolejko, *Phys. Rev.* **D83**, 083503 (2011).
[21] A. Krasiński, *Phys. Rev.* **D84**, 023510 (2011).
[22] A. Krasiński, *Phys. Rev.* **D86**, 064001 (2012).
[23] P. Szekeres, in: *Gravitational Radiation, Collapsed Objects and Exact Solutions*. Edited by C. Edwards. Springer (Lecture Notes in Physics, vol. 124), New York, pp. 477 – 487 (1980).
[24] C. Hellaby and K. Lake, *Astrophys. J.* **282**, 1 1984) + erratum *Astrophys. J.* **294**, 702 (1985).
[25] R. McMahon, Quasars and Galaxies at the Highest Redshifts. Crafoord Symposium 2005, http://powershow.com/view/24faaf-OTQ2Y/Quasars_and_Galaxies_at_the_Highest_Redshifts_powerpoint_ppt_presentation
[26] M. Luciuk, Astronomical Redshift, http://www.asterism.org/tutorials/tut29-1.htm, last updated 2004.
[27] http://www.asknumbers.com/LengthConversion.aspx
[28] M. L. McClure, C. Hellaby, *Phys. Rev.* **D78**, 044005 (2008).
[29] J. Zibin, *Phys. Rev.* **D84**, 123508 (2011); *Phys. Rev.* **D78**, 043504 (2008); also private communication from the anonymous referees of Ref. [7].
[30] P. Szekeres, *Commun. Math. Phys.* **41**, 55, (1975).
[31] J. Silk, *Astron. Astrophys.* **59**, 53 (1977).
[32] S. W. Goode and J. Wainwright, *Phys. Rev.* **D26**, 3315, (1982).
[33] P. Bull, T. Clifton, P. G. Ferreira, *Phys. Rev.* **D85**, 024002 (2012).
[34] K. Bolejko, *Phys. Rev.* **D73**, 123508 (2006).
[35] K. Bolejko, *Phys. Rev.* **D75**, 043508 (2007).
[36] K. Bolejko, *Gen. Relativ. Gravit.* **41**, 1585 (2009).
[37] K. Bolejko, *Gen. Relativ. Gravit.* **41**, 1737 (2009).
[38] K. Bolejko, M.-N. Célérier, *Phys. Rev.* **D82**, 103510 (2010).
[39] K. Bolejko and R. A. Sussman, *Phys. Lett.* **B697**, 265 (2011).
[40] K. Bolejko, *Astron. Astroph.* **525**, A49 (2011).
[41] K. Bolejko, C. Clarkson, R. Maartens, D. Bacon, N. Meures and E. Beynon, *Phys. Rev. Lett.* **110**, 021302 (2013).
[42] A. Krasiński and C. Hellaby, *Phys. Rev.* **D69**, 023502 (2004).
[43] K. Bolejko, A. Krasiński and C. Hellaby, *Mon. Not. Roy. Astr. Soc.* **362**, 213 (2005).
[44] A. A. Friedmann, *Z. Physik* **10**, 377 (1922); reprinted as a Golden Oldie in *Gen. Relativ. Gravit.* **31**, 1985 (1999) + addendum: *Gen. Relativ. Gravit.* **32**, 1937 (2000).